Electronic Supplementary Information for Mining Predicted Crystal Structure Landscapes with High Throughput Crystallisation: Old Molecules, New Insights

Peng Cui[1], David P. McMahon[2], Peter R. Spackman[2,3], Ben M. Alston[1,3], Marc A. Little[1], Graeme M. Day*[2] and Andrew I. Cooper*[1,3]

[1]Department of Chemistry and Materials Innovation Factory, University of Liverpool, Liverpool, L7 3NY, UK.

[2]Computational Systems Chemistry, School of Chemistry, University of Southampton, SO17 1BJ, UK.

[3]Leverhulme Research Centre for Functional Materials Design, Department of Chemistry and Materials Innovation Factory, University of Liverpool, Liverpool, L7 3NY, UK.

This PDF file includes:

Materials and Methods

Figures S1 to S41.

Tables S1 to S10.

Table of Contents:

1.0 Computational Methodology

Molecular conformers were generated via a conformation search in the Schrödinger Maestro package using the OPLS2005[1] force field (no cut off and a dielectric constant of 1.0) using a mixed torsional/low-mode search. A maximum of 10000 steps were allowed and conformers with an energy less than 35 kJ mol^{-1} from the global minimum and with an RMSD in atomic positions of greater than 0.3 Å from all previously generated conformers were retained. Each conformer was subsequently geometry optimized using dispersion corrected (D3BJ[2]) density functional theory (DFT), using the B3LYP[3-4] functional with a 6-311G(d,p)[5-6] basis. Molecular DFT calculations were performed with the Gaussian09 software (Revision D).[7] Redundant conformers (again, those with an RMSD < 0.3 Å) according to their DFT optimized gas-phase geometries were then eliminated. These gas-phase molecular geometries were then held rigid throughout crystal structure generation and lattice energy minimization.

When optimising gas-phase molecular conformations, two unique conformers for **TMA** were found at the aforementioned DFT level, and six conformers were found for **ADTA**. The lowest energy conformer was **TMA1**, which has 3-fold rotational symmetry, with the **TMA2** conformer (flipping the orientation of one proton on the carboxylic acid group) sitting 1.003 kJ/mol higher in intramolecular energy, as show in Figure S1 below. **ADTA2** was the lowest energy conformer, with the relative energies for **ADTA1**, **ADTA3**, **ADTA4**, **ADTA5** and **ADTA6** being 2.767, 0.346, 1.763, 2.046 and 2.399 kJ/mol respectively. The only significant differences in **ADTA** conformers were relative rotations of the carboxylic acid groups.

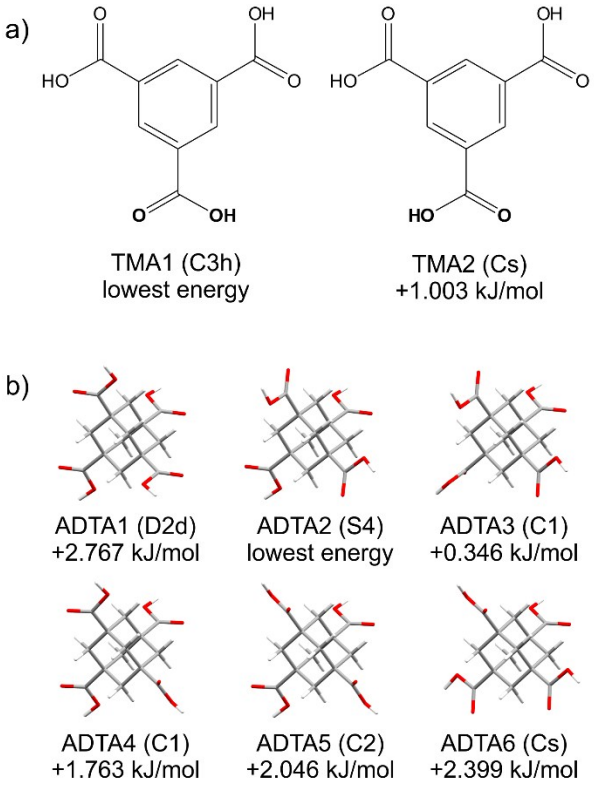

Figure S1. a) Two-dimensional schematics for the **TMA1** and **TMA2** conformers, showing the only change in a single carboxylic acid group. b) Conformers of **ADTA**. Points groups of all conformers are given in parentheses and calculated energies relative to the lowest energy conformer in the gas phase.

Crystal Structure Prediction (CSP) was then performed using a quasi-random sampling procedure, as implemented in the Global Lattice Energy Explorer software (version 2).[8] For both TMA and ADTA, trial crystal structures were generated with a single molecule as the asymmetric unit in each of the 25 most frequently observed space groups, as determined by statistics gathered from examination of non-polymeric $Z' = 1$ organic molecular crystal structures reported in the Cambridge Structure Database (CSD).[9] For reference, the international tables of crystallography numbers for these space groups were: 61, 14, 19, 2, 4, 15, 33, 9, 29, 5, 1, 60, 7, 18, 96, 76, 145, 43, 56, 13, 169, 88, 20, 86, and 148. A target of 10,000 valid optimized structures per space group (per conformer) was used (250,000 crystal structures per conformer). Crystal structure searches were also performed with two independent molecules in the asymmetric unit ($Z'= 2$) for **TMA**, with the three combinations of the two conformers. These $Z'= 2$ searches were performed in the 7 most frequently observed space groups (1, 2, 4, 14, 15, 19 and 61) and a total of 180,000 valid optimized crystal structures were generated for each combination of conformers, distributed as: 50,000 in each of space groups 14 and 15; 25,000 in each of space groups 4 and 61; 10,000 in each of space groups 1, 2 and 19.

Initial crystal generation involved a low-discrepancy sampling of all structural variables within each space group: unit cell lengths and angles, and molecular positions and orientations within the asymmetric unit. Space-group symmetry was then applied, and a geometric test was performed for overlap between molecules. Molecular clashes (e.g. overlapping molecules) were removed by lattice expansion, using the separating axis theorem. For each generated structure, a series of rigid lattice-energy minimizations were performed. All lattice energy calculations in this procedure were performed with an anisotropic atom–atom potential using DMACRYS2.3.0.[10] Electrostatic interactions were modelled using an atomic multipole description of the molecular charge distribution (up to hexadecapole on all atoms) from the B3LYP/6-311G(d,p) -calculated charge density using distributed multipole analysis via GDMA (version 2).[11] Atom–atom repulsion and dispersion interactions were modelled using the FIT intermolecular potential.[12] Charge–charge, charge–dipole and dipole–dipole interactions were calculated using Ewald summation; all other intermolecular interactions were summed to a 25 Å cut-off between molecular centres-of-mass, with the cut off for interactions reduced smoothly to 27 Å using a spline.

For each generated crystal structure, multiple (3) rigid lattice energy minimizations were performed. During the initial lattice energy minimization point-charges obtained using MULFIT[13] to fit atomic charges to the molecular electrostatic potential generated by the B3LYP/6-311G**-distributed multipole analysis atomic multipoles were used in conjunction with a pressure of 0.1 GPa, and the van der Waals cut off increased by 10 Å. For all subsequent steps, multipoles at the hexadecapole level were used without pressure. Minimization cycles were continued until at least 3 minimizations had been performed and the structure had reached a minimum (as indicated by an F-value < 1, where F summarizes changes in unit cell lengths, angles, molecular positions and orientations during lattice energy minimization).

Final, total energies of each predicted crystal structure were calculated as the sum of the intermolecular interaction energy calculated in DMACRYS and the conformational energy of the conformer in the crystal structure, relative to the lowest energy gas phase conformer.

Redundant crystal structures from each CSP were eliminated by through comparison of predicted powder X-ray diffraction (PXRD) patterns. Predicted powder patterns were calculated using PLATON.[14] Each structure was compared to all other structures in an energy & density window (within 1 kJ/mol & 0.05 g/cm^3) of the reference structure, and powder patterns (calculated with wavelength 0.7 Å restricted to the two-theta range of [0,20], with bin widths of 0.02 degrees) were compared using constrained dynamic time warping (CDTW), taking the minimum distance of all steps 0-10. Patterns were normalized such that their area under the curve was unity. Structures within the aforementioned energy window, with powder pattern differences calculated to be less than 1.0 by CDTW were considered identical. Structures were compared within all space groups for each conformer, and for TMA structures between the $Z' = 1$ and $Z' = 2$ structures for each conformer (but not the $Z' = 2$ structures with both conformers).

The energies for the previously found experimental structures **BTCOAC**[24] and **TMA-γ**[37] (CSD entry codes 1115589 and 1841046 respectively) were calculated by taking the experimental structures, reducing the space group symmetry to P1 (i.e. taking the asymmetric units to be 48 and 24 molecules respectively) and manually placing hydrogens on one of the two positions available for each molecule depending on neighbouring hydrogen-bonded molecules. Each molecule in the unit cell was subsequently optimised using Gaussian09 (with the same settings as the CSP structures) while constraining the dihedral angles between the oxygen atoms and the plane of the aromatic ring. These constrained geometries were then subjected to the periodic boundary conditions and the lattice energies minimized using DMACRYS with the same methods and parameters described for the CSP. This provides an estimated lattice energy that would have been found had our search space for the CSP included these structures. Conformational (intramolecular) energies of the molecules were all less than 7.5 kJ/mol from that of **TMA1**, and these were utilised to adjust the lattice energies accordingly.

1.1 Classification of predicted crystal structures

All predicted **TMA** crystal structures were classified according to the presence of hexagonal hydrogen bonded rings, which are the basic structural unit of the hexagonal hydrogen bonded layers in the observed (α and γ) crystal structures. This classification was performed by searching all crystal structures against a reference idealized, planar hydrogen bonded hexamer (Figure S1). Only non-hydrogen atoms were included in the search, to allow for any **TMA** conformer within the rings, and loose geometric tolerances (± 40% in interatomic distances and ± 30 degrees in interatomic angles) to allow for non-planar hexamers and hexamers without perfect double hydrogen bonds between each molecule. These searches were performed using the Mercury crystal structure analysis program.

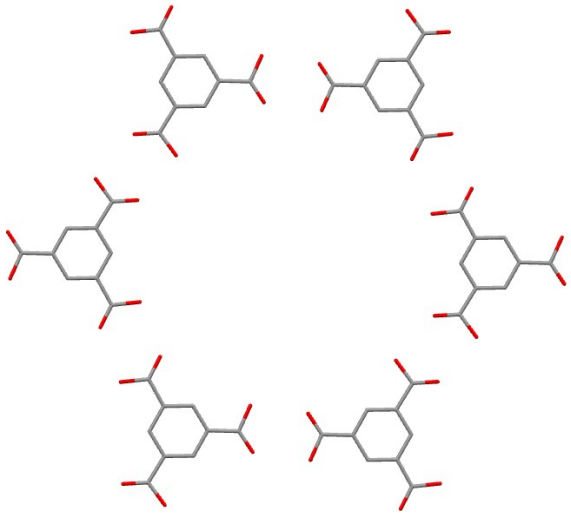

Figure S2. **TMA** hydrogen bonded hexamer used as reference for searching against predicted crystal structures.

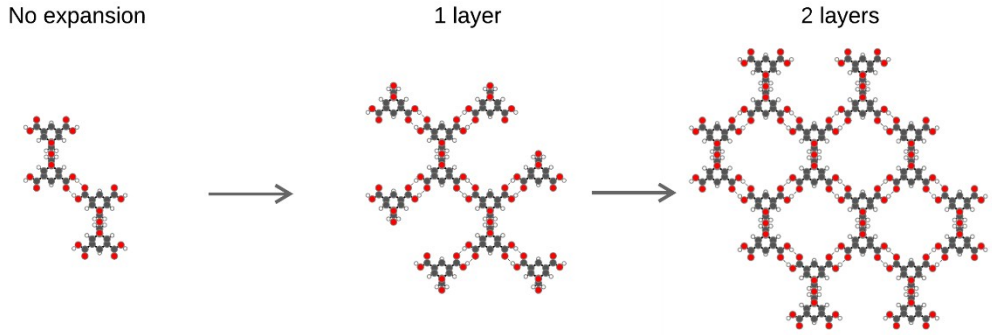

Figure S3. Single diamondoid lattice from **ADTA** before expansion, after 1 layer and 2 layers. Each of these lattices in each crystal structure was expanded for analysis to determine degree of lattice interpenetration.

All predicted **ADTA** crystal structures were analysed according to their hydrogen bond networks and degree(s) of interpenetration these lattices within each crystal structure. This classification was performed by expanding a cluster of molecules consisting of all hydrogen-bonded molecules to each molecule in the unit cell and neighbouring cells, then repeating this process on the cluster 4 times (Figure S2 shows a visual representation of this process for the first 2 steps on a single lattice). The resulting connectivity graph consisting of covalent and hydrogen bonds was then analysed for subgraphs (or connected components), with the number of these distinct subgraphs which passed through the unit cell providing the degree of lattice interpenetration. Hydrogen bonds were classified according to the sum of van der Waals radii along with D…H…A angle being greater than 160 degrees. Custom code was written for this purpose. For the resulting plot, only those displaying a diamondoid network were coloured by their number of distinct hydrogen bonded networks, as determined by each molecule in the unit cell being hydrogen bonded to exactly 4 neighbouring molecules.

2.0 Materials and Methods

2.1 General Methods

All chemicals and solvents were obtained from Sigma-Aldrich, TCI Europe, Fisher, Manchester Organics, Alfa Aesar, Combi-Blocks, and Jilin Province Yanshen Technology Co., Ltd. All chemicals and solvents were used as received. Anhydrous solvents were purchased from Sigma-Aldrich or Acros Organics and used without further purification. All gases for sorption analysis were supplied by BOC at a purity of ≥99.999%.

2.1.1. Robot Configuration

A Chemspeed SWING POWDERDOSE robotic platform equipped with both solid and liquid dispensing tools (Figure S4) was used in HT crystallisation procedure. Liquid handling was carried out via a four needle overhead dispensing tool powered by 4 syringe pumps (syringe volumes: 1, 10 or 25 ml). After each dispense, the syringe was washed with ethanol for next dispensing. HT Crystallisations were carried out in standard 8 ml glass vials, held in removable racks (80 vials in a 16 x 5 array). The dispensing was carried at RT in a closed hood system.

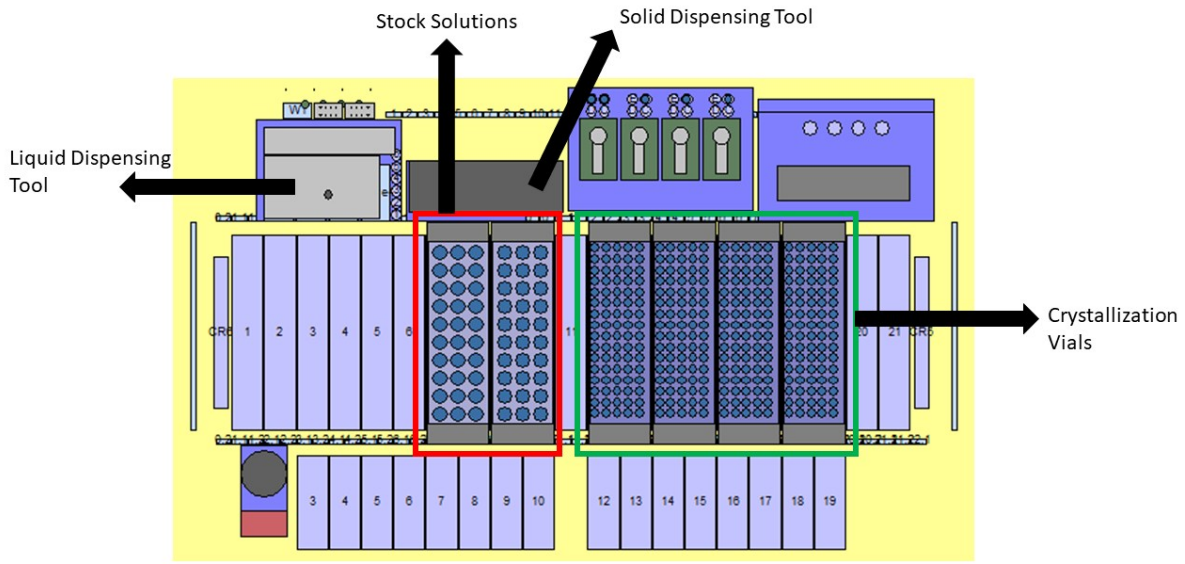

Figure S4. Chemspeed SWING POWDERDOSE robotic platform setup for HT crystallisation experiment.

2.1.2. Powder X-ray Diffraction (PXRD)

For screening purposes, PXRD patterns were collected in transmission mode on samples held on thin Mylar film in aluminium well plates on a Panalytical Empyrean diffractometer, equipped with a high throughput screening XYZ stage, X-ray focusing mirror, and PIXcel detector, using Cu-Kα (λ = 1.541 Å) radiation. Unless stated, PXRD patterns were recorded at room temperature. Diffraction patterns were measured over the 2θ range 2−40°, in 0.013° steps, for 15-30 minutes. For PXRD data collected using samples suspended in solvent, for variable temperature *in situ* experiments, and for indexing purposes, samples were loaded into borosilicate glass capillaries which were spun during data collections to improve powder averaging. PXRD data for these samples were recorded in transmission mode on a Panalytical Empyrean diffractometer, equipped with a sample spinner, X-ray focusing mirror, and PIXcel

detector, using Cu-Kα (λ = 1.541 Å) radiation. For the variable temperature experiments, sample temperatures were controlled using an Oxford Cryosystems 700 series cryostream. High resolution synchrotron PXRD data for **ADTA_2-2**, was collected using the I11 beamline at Diamond Light Source (λ = 0.825186 Å), which is equipped with a Mythen II position sensitive detector. This sample was loaded in a borosilicate glass capillary that was spun to improve powder averaging during data acquisition and the sample was heated using an Oxford Hot-Air-Blower. PXRD patterns were indexed by Le Bail fitting in TOPAS-Academic.[15]

2.1.3. Single Crystal X-ray Diffraction (SC-XRD)

SC-XRD data sets were measured on a Rigaku MicroMax-007 HF rotating anode diffractometer (Mo-Kα radiation, λ = 0.71073 Å, Kappa 4-circle goniometer, Rigaku Saturn724+ detector); or at beamline I19, Diamond Light Source, Didcot, UK using silicon double crystal monochromated synchrotron radiation (λ = 0.6889 Å, Pilatus 2M detector). Rigaku frames were converted to Bruker compatible frames using the programme ECLIPSE.[16] Absorption corrections, using the multi-scan method, were performed with the program SADABS.[17-18] For synchrotron X-ray data, collected at Diamond Light Source (λ = 0.6889Å) data reduction and absorption corrections were performed with xia2.[19] Structures were solved with SHELXT,[20] or by direct methods using SHELXS,[21] and refined by full-matrix least squares on $|F|^2$ by SHELXL,[22] interfaced through the programme OLEX2.[23] Attempts were made to locate H-atom positions for all the carboxylic acid OH groups, however, due to disorder this was not possible. When this was not possible, OH group were refined using the riding model. All other H-atoms were fixed in geometrically estimated positions and refined using the riding model. During refinement, all **TMA** and **ADTA** non-hydrogen molecules were refined anisotropically. In addition, solvent molecules which were reasonably well ordered were refined anisotropically with H-atoms. For the following crystal structures; **TMA_2-33**, **TMA_7-35**, **TMA_8-32**, **TMA_8-35**, **ADTA_2-27**, **ADTA_2-35**, it was not possible to resolve solvent molecules in the large lattice voids. To avoid using solvent masks during the refinement of these crystal structure, disordered solvent was modelled exclusively as disordered O-atoms, without riding H-atoms. For displacement ellipsoid plots from all the single crystal structure, see Figure S43.

2.1.4 NMR

NMR spectra were recorded on a Bruker 400 NMR spectrometer at 400 MHz (^{1}H) and 100 MHz (^{13}C) and referenced against the residual ^{1}H or ^{13}C signal of the solvent.

2.1.5 TGA

Thermogravimetric analysis was carried out using a TA Q5000IR analyzer with an automated vertical overhead thermobalance. Samples were heated at a rate of 10 °C/min unless otherwise stated.

2.1.6 Gas Sorption Analysis

Surface areas were measured by nitrogen sorption at 77.3 K. Powder samples were degassed on the analysis port under vacuum. Isotherm measurements were performed using a Micromeritics 3flex surface characterization analyzer, equipped with a Cold-Edge technologies

liquid helium cryostat chiller unit for temperature control. High pressure CO_2 isotherms were recorded up to a pressure of 10 bar, at 273 K, using a Micromeritics ASAP 2050 xtended pressure sorption analyzer.

2.2 HT crystallisation for TMA

2.2.1 TMA solubility test

General method: 44 organic solvents were used for the solvent library (Table S1). Initially, these solvents were used to determine the solubility of the target compound using the general protocol: 1 mL of organic solvent was added to a sample vial containing **TMA** (~ 5 mg). The vial was then agitated at room temperature and if the **TMA** fully dissolved, more **TMA** was added in ~ 1 mg portions. The solubility of **TMA** in each solvent was calculated in terms of mg/mL. The organic solvents which dissolved ≥ 15 mg/mL of **TMA**, at room temperature, and which had boiling points below 120 °C, were chosen as good solvents for the HT crystallisation screen for **TMA** (Table S2).

Table S1. Solvents for the experimental crystallisation screen.

diethyl ether	*n*-pentane	dichloromethane (DCM)	acetone	methyl acetate	chloroform
methanol	tetrahydrofuran (THF)	diisopropyl ether	*n*-hexane	1,3-dioxolane	ethyl acetate
trifluoroethanol	ethanol	hexafluorobenzene	cyclohexane	acetonitrile(MeCN)	2-propanol
tetrahydropyran	1,4-difluorobenzene	1-propanol	*n*-heptane	1,4-dioxane	toluene
1-butanol	tetrachloroethylene	*o*-xylene	*m*-xylene	*p*-xylene	triethylorthoformate
N,*N*-dimethylformamide (DMF)	cyclohexanone	mesitylene	dimethylacetamide (DMA)	*N*,*N*-diethylformamide (DEF)	*n*-butylbenzene
dimethyl sulfoxide (DMSO)	1-methyl-2-pyrrolidinone (NMP)	γ- butyrolactone	1,2-dimethoxybenzene	1,3-dimethoxybenzene	diphenyl ether
isooctane	tetradecane				

Solubility results:

For **TMA**, we determined that there are eight organic solvents, with boiling point < 120 °C, which dissolved **TMA** at a concentration of ≥ 15mg/mL. The order of increased solubility of **TMA** in these solvents was determined to be: THF > ethanol > methanol > 1,4-dioxane > tetrahydropyran > 1-propanol, 2-propanol, and 1-butanol. We also determined that there are six solvents with boiling points > 120 °C, which dissolved **TMA** at a concentration of ≥ 5 mg/mL, these are, DMF, DMA, DEF, DMSO, NMP and γ- butyrolactone.

The eight 'good solvents'; THF, ethanol, methanol, 1,4-dioxane, tetrahydropyran, 1-propanol, 2-propanol, and 1-butanol, were used to prepare 15 mg/mL stock solutions of **TMA** for the HT crystallisation screen. The solvents with higher boiling points (> 120 °C) were not used for the HT crystallisation screens, as it can be problematic to evaporate these solvents at room temperature, which may have prevented **TMA** from crystallising during this study. All of

solvents, which did not dissolve **TMA** at a concentration ≥ 15 mg/mL, were used bad solvents for the HT crystallisation experiment.

2.2.2 HT crystallisation experiment

For the HT crystallisation screen, stock solutions of **TMA** (1.5 g, 7 mmol) in organic solvent (100 mL), were prepared in each of the eight 'good solvents' (THF, ethanol, methanol, 1,4-dioxane, tetrahydropyran, 1-propanol, 2-propanol, and 1-butanol), at room temperature. For each crystallisation, a 1 mL portion of the **TMA** stock solution was transferred into 36 different sample vials, loaded in racks on the Chemspeed platform at room temperature. A 1 mL portion of the of the 36 other solvents (1-36) listed in Table S2 were then added into these vials, to form 1:1 (*v*:*v*) binary solvent mixtures. The process was repeated with the seven other 'good solvent' stock solutions. After mixing, the crystallisation solvents were then allowed to evaporate from the uncapped sample vials at room temperature, over several days, or weeks, resulting in crystallisation of **TMA**.

Table S2. Solvents used during the HT crystallisation screening. The solvents are numbered 1-38 and these numbers are used through the manuscript and SI.

1. methanol	2. THF	3. ethanol	4.2-propanol	5.tetrahydropyran	6. 1-propanol
7. 1,4-dioxane	8. 1-butanol	9. diethyl ether	10. *n*-pentane	11. DCM	12. acetone
13. methyl acetate	14. chloroform	15.diisopropyl ether	16. *n*-hexane	17. 1,3-dioxolane	18. ethyl acetate
19.trifluoroethanol	20.hexafluorobenzene	21.cyclohexane	22.acetonitrile	23. 1,4-difluorobenzene	24. *n*-heptane
25. toluene	26.tetrachloroethylene	27. *o*-xylene	28. *m*-xylene	29. *p*-xylene	30.triethylorthoformate
31.cyclohexanone	32. mesitylene	33. *n*-butylbenzene	34. 1,2-dimethoxybenzene	35. 1,3-dimethoxybenzene	36. diphenyl ether
37. isooctane	38. tetradecane				

For the HT crystallisation screens, we used the following sample labelling scheme:

TMA_[good solvent number]-[other solvent number].

Hence, if the 'good solvent' was ethanol (#3), and the other solvent was acetone (#12), the following sample code was used: **TMA**_3-12.

2.2.3 Sample transfer

After several days, or up to a few weeks after mixing the solvents, the **TMA** samples had crystallised from the organic solvent mixtures. The crystalline material was then isolated by filtration, or transferred directly into a HT PXRD plate, without any further sample preparation. Approximately 10 mg of **TMA** was used during the HT PXRD measurement. At this stage, no other information, regarding crystal size or morphology, was determined for the samples.

For **TMA**, experimental PXRD patterns were screened alongside the simulated PXRD pattern of the predicted low density polymorph, **1**, and the simulated PXRD patterns for the **TMA** structures reported in the Cambridge Crystallographic Data Centre (CCDC) and the literature (Table S3). Samples were initially screened on the basis of observed peak position, rather than peak intensity, as powdered samples were not carefully prepared. The general method used here is shown in Figure S4. Here, the PXRD patterns of the different samples were compared to simulated PXRD pattern of the predicted low-density polymorph, **1**, as well as the simulated PXRD patterns of the known **TMA** structures. Where obvious differences were observed, attempts were made to determine the structures obtained from these crystallisation conditions using SC-XRD.

2.3 HT crystallisation for adamantane-1,3,5,7-tetracarboxylic acid (ADTA)

2.3.1 ADTA solubility test

Initially, 1 mL of organic solvent was added to **ADTA** (~ 3 mg) in a sample vial, at room temperature. If the **ADTA** fully dissolved, more **ADTA** was added in ~ 1 mg portions and total amount of **ADTA** added to the vial was recorded. The solubility of **ADTA** in each solvent was calculated in terms of mg/mL. The organic solvents which dissolved ≥ 3 mg/mL of **ADTA**, and which had boiling points < 120 °C, were chosen as 'good solvents' for the HT crystallisation screen with **ADTA**. The order of increased solubility of **ADTA** in these solvents was determined to be: methanol > THF, ethanol > 1,4-dioxane > 2-propanol > 1-propanol.

The six 'good solvents'; methanol, THF, ethanol, 1,4-dioxane, 2-propanol, 1-propanol, were used to prepare 3 mg/mL stock solutions of **ADTA** for the HT crystallisation screen. All of solvents, which did not dissolve **ADTA** at a concentration ≥ 3 mg/mL, were used as bad solvent for the HT crystallisation experiment.

2.3.2 HT crystallisation experiment

For the HT crystallisation screen, stock solutions of **ADTA** (0.3 g, 0.96 mmol) in organic solvent (100 mL), were prepared in each of the six 'good solvents' (methanol, THF, ethanol, 1,4-dioxane, 2-propanol, 1-propanol), at room temperature. For each crystallisation, a 2 mL portion of the **ADTA** stock solution was transferred into 38 different sample vials, loaded in racks on the Chemspeed platform, at room temperature. A 2 mL portion the 38 solvents listed in Table S2 were then added into these vials, to form 37 1:1 (*v*:*v*) binary solvent crystallisation, and 1 single solvent crystallisation. The process was repeated for all five other 'good solvent' stock solutions. After mixing, the crystallisation solvents were then allowed to evaporate from the uncapped sample vials at room temperature, over several days, or weeks, resulting in crystallisation of **ADTA**. Sample transfer and data collection were carried out as described in Section 2.2.3.

Table S3. Previously reported **TMA** crystal structures.

Name	Solvent	Space group	*a* (Å)	*b* (Å)	*c* (Å)	*α* (°)	*β* (°)	*γ* (°)	*V* (Å^3)	Reference
1115589		*C*2/*c*	26.52	16.42	26.55		91.53		11557.70	[24]
1137091	acetone	*C*2/*c*	26.54	16.48	26.60		92.65		11625.40	[25]
204677	DMF	$P2_1/c$	16.65	14.41	7.23		90.72		1735.59	[26]
696617	DMSO	$P2_1/m$	8.74	6.84	10.71		96.19		636.59	[27]
856377	DMSO	*Pnma*	18.91	21.09	5.28				2104.97	[28]
274617	$2H_2O$	$Pna2_1$	21	13.34	3.69				1032.91	[29]
1275695	$0.83(H_2O)$	*P*1	16.64	18.55	9.51	95.81	91.06	94.35	2911.26	[30]
112933	MeOH_H_2O	$P\bar{1}$	3..70	8.97	18.04	77.76	86.86	88.04	580.77	[31]
670472	heptanol	$P\bar{1}$	8.25	8.47	11.98	94.37	104.87	110.39	745.69	[32]
670473	butanol	$P\bar{1}$	9.05	9.06	9.29	63.16	88.49	83.96	675.90	[32]
670474	hexanol	$P\bar{1}$	8.28	8.62	12.00	104.20	93.13	110.89	765.37	[32]
1272474	dioxane	$P\bar{1}$	9.53	9.54	8.03	89.68	95.01	92.03	726.37	[33]
233070	MeOH	$P\bar{1}$	7.88	8.96	8.96	111.93	96.72	110.57	526.24	[34]
233071	2MeOH	$P\bar{1}$	3.75	9.58	17.73	91.21	91.88	94	635.21	[34]
1841046	HAc	*I*222	24.223	15.332	16.531				6139.4	[35]
2**TMA**_pyrene_2ethanol		*C*2/*c*	28.13	16.55	14.73		95.13		6827	[36]
2**TMA**_n-tetradecane		$P3_1$ or $P3_2$	16.5	16.5	10.07					[37]
2**TMA**_isooctane		*C*2/*c*	28.60	16.60	6.93		102.55			[37]
2**TMA**_CRO_2H2O		$P\bar{1}$	7.50	8.02	14.71	77.05	79.48	84.41	846.69	[38]
2**TMA**_HEL		*C*2/*c*	23.07	16.18	9.15		92.83		3411.1	[39]

Table S4. Previously reported **ADTA** crystal structures.

Name	**Space group**	***a* (Å)**	***b* (Å)**	***c* (Å)**	***α* (°)**	***β* (°)**	***γ* (°)**	***V* (Å^3)**	**Reference**
1165614	$I4_1/a$	7.510		22.266				1255.8	[40]

3.0 Supplementary Data

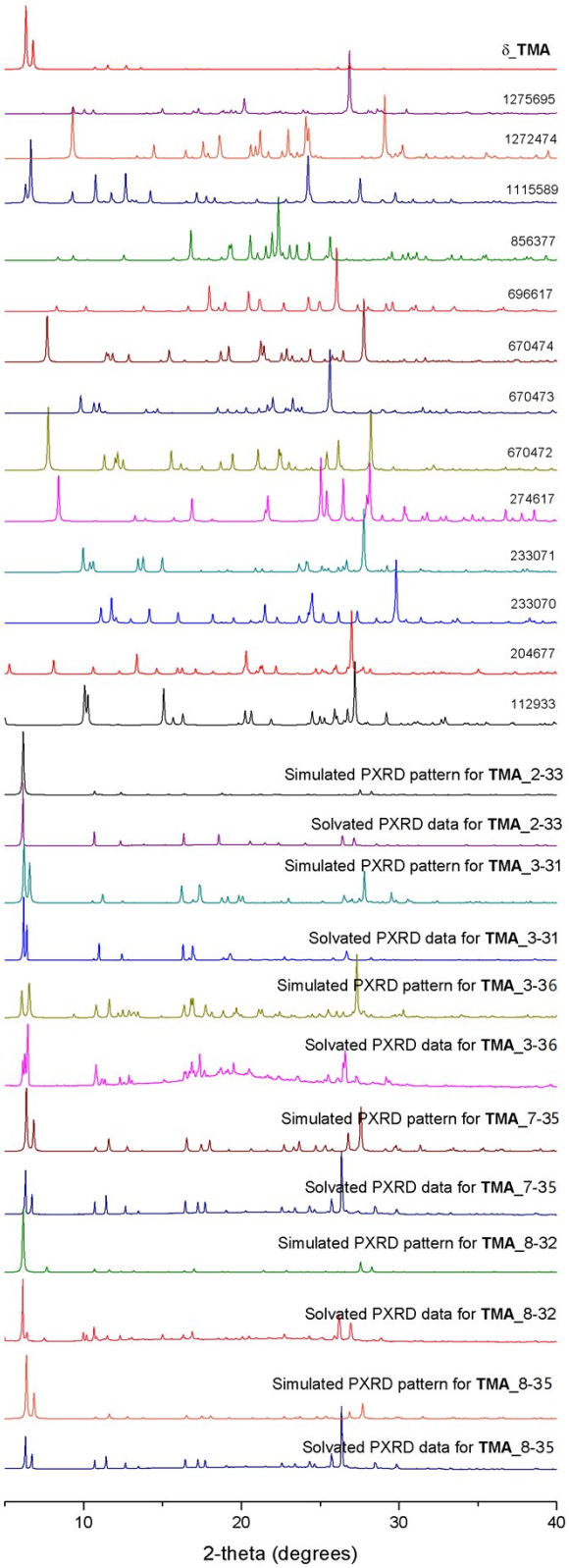

Figure S5. Simulated PXRD pattern of the predicted low-density polymorph, **1** (top, red) above the simulated PXRD patterns of the previously reported **TMA** structures shown in Table S3, and the solvated data for the experimental hits from the HT crystallisation screen, which we characterised using SC-XRD.

Table S5. Single crystal X-ray refinement details for **TMA** solvated structures.

	TMA_3-36	**TMA_3-31**	**TMA_2-33**
Crystallisation Solvent	EtOH / Ph_2O	EtOH / cyclohexanone	THF / *n*-butylbenzene
Space Group	$P\bar{1}$	*C*2/*c*	$P3_121$
Wavelength [Å]	0.6889 Å	Mo-Kα	Mo-Kα
Collection Temperature	200 K	100 K	100 K
Formula	$3(C_9H_6O_6)\cdot2(C_{12}H_{10}O)$	$C_9H_6O_6\cdot C_6H_{10}O$	$C_9H_6O_6\cdot2(H_2O)$
Mr	970.81	308.28	246.17
Crystal Size (mm)	0.078 x 0.028 x 0.024	0.085 x 0.058 x 0.047	0.134 x 0.063 x 0.039
Crystal System	Triclinic	Monoclinic	Trigonal
a [Å]	10.50240(6)	27.254(3)	16.5141(6)
b [Å]	15.88590(7)	16.7260(16)	
c [Å]	16.60930(7)	6.7365(6)	9.7096(4)
α [°]	113.7260(4)		
β [°]	98.4480(4)	100.207(3)	
γ [°]	106.8020(4)		
V [Å^3]	2316.46(2)	3022.2	2293.20(19)
Z	2	8	6
D_{calcd} [g cm^{-3}]	1.392	1.355	1.070
μ [mm^{-1}]	0.100	0.109	0.097
F(000)	1008	1296	768
2θ range [°]	2.72 – 56.30	2.87 – 52.90	5.07 – 52.74
Reflections collected	36998	16923	24980
Independent reflections, R_{int}	12320, 0.0281	3117, 0.0463	3095, 0.0516
Obs. Data [$I > 2\sigma$]	8999	2261	2533
Data / restraints / parameters	12320 / 196 / 700	3117 / 116 / 257	3095 / 6 / 174
Final R1 values ($I > 2\sigma(I)$)	0.0429	0.0731	0.0638
Final R1 values (all data)	0.0559	0.0943	0.0740
Final wR(F^2) values (all data)	0.1429	0.2492	0.2217
Goodness-of-fit on F^2	1.100	1.065	1.062
Largest difference peak and hole [e.A^{-3}]	0.306 / -0.380	0.767 / -0.485	0.405 / -0.272
CCDC	1915309	1915304	1915315

Table S6. Single crystal X-ray refinement details for **TMA** solvated structures.

	TMA_8-35	**TMA_7-35[a]**	**TMA_8-32[b]**
Crystallisation Solvent	1-Butanol / 1,3-dimethoxybenzene	1,4-dioxane / 1,3-dimethoxybenzene	1-Butanol / mesitylene
Space Group	*C*2/*m*	*C*2/*m*	$P3_221$
Wavelength [Å]	Mo-Kα	Mo-Kα	Mo-Kα
Collection Temperature	100 K	100 K	100 K
Formula	$C_9H_6O_6 \cdot 5.4(H_2O)$	$C_9H_6O_6 \cdot 7.5(O)$	$2(C_9H_6O_6) \cdot 8(O)$
Mr	296.14	330.14	548.28
Crystal Size (mm)	0.021 x 0.011 x 0.01	0.017 x 0.011 x 0.009	0.015 x 0.013 x 0.009
Crystal System	Monoclinic	Monoclinic	Trigonal
a [Å]	25.768(4)	25.869(4)	16.5230(16)
b [Å]	16.425(2)	16.419(3)	
c [Å]	3.6006(5)	3.6060(6)	19.400(2)
α [°]			
β [°]	93.333(4)	93.617(4)	
γ [°]			
V [Å^3]	1521.3(4)	1528.6(4)	4586.9(10)
Z	4	4	6
D_{calcd} [g cm^{-3}]	1.340	1.435	1.191
μ [mm^{-1}]	0.125	0.143	0.113
F(000)	647.0	672	1680
2θ range [°]	4.96 – 52.90	4.96 – 54.99	4.94 – 52.26
Reflections collected	8267	1664	1680
Independent reflections, R_{int}	1618, 0.521	1664, 0.0431	55344, 0.0919
Obs. Data [$I > 2\sigma$]	1293	1533	3656
Data / restraints / parameters	1618 / 0 / 115	1664 / 1 / 137	6239 / 230 / 363
Final R1 values ($I > 2\sigma(I)$)	0.0887	0.0688	0.0777
Final R1 values (all data)	0.1014	0.0727	0.1344
Final wR(F^2) values (all data)	0.2458	0.2049	0.2266
Goodness-of-fit on F^2	1.785	1.070	0.981
Largest difference peak and hole [e.A^{-3}]	0.588 / -0.433	0.317 / -0.415	0.379 / -0.312
CCDC	1915314	1915308	1915313

[a] X-ray data was integrated and scaled as a two-component twin using TWINABS and the X-ray crystal structure was refined with a HKLF 5 reflection file format. [b] The X-ray crystal structure was refined with the TWINLAW [$\bar{1}00$ $0\bar{1}0$ 001] and BASF refined to 0.459; the X-ray data quality for this structure was poor and a RIGU restraint was used during refinement.

Table S7. Single crystal X-ray refinement details for **TMA** solvated structures.

	TMA_4-18	**TMA_6-18**
Crystallisation Solvent	2-propanol / ethyl acetate	1-propanol / ethyl acetate
Space Group	*C*2/*c*	$P\bar{1}$
Wavelength [Å]	Mo-Kα	Mo-Kα
Collection Temperature	100 K	100 K
Formula	$C_9H_6O_6 \cdot (C_3H_8O)$	$C_9H_6O_6 \cdot (C_3H_8O)$
Mr	270.23	270.23
Crystal Size (mm)	0.188 x 0.101 x 0.079	0.408 x 0.315 x 0.079
Crystal System	Monoclinic	Triclinic
a [Å]	19.0126(17)	9.1671(17)
b [Å]	9.6004(8)	9.4589(18)
c [Å]	27.383(2)	9.6179(17)
α [°]		93.220(5)
β [°]	90.563(2)	116.280(5)
γ [°]		118.728(5)
V [Å^3]	4998.0(8)	616.2(2)
Z	8	2
D_{calcd} [g cm^{-3}]	1.437	1.457
μ [mm^{-1}]	0.120	0.121
F(000)	2272	284
2θ range [°]	2.97 – 52.89	5.026 – 62.278
Reflections collected	23878	8579
Independent reflections, R_{int}	5145, 0.0488	3929, 0.0833
Obs. Data [$I > 2\sigma$]	4122	2510
Data / restraints / parameters	5145 / 3 / 373	3929 / 3 / 189
Final R1 values ($I > 2\sigma(I)$)	0.0564	0.0486
Final R1 values (all data)	0.0687	0.0759
Final wR(F^2) values (all data)	0.1624	0.12030
Goodness-of-fit on F^2	1.036	0.912
Largest difference peak and hole [e.A^{-3}]	0.651 / -0.317	0.302 / -0.330
CCDC	1915311	1915310

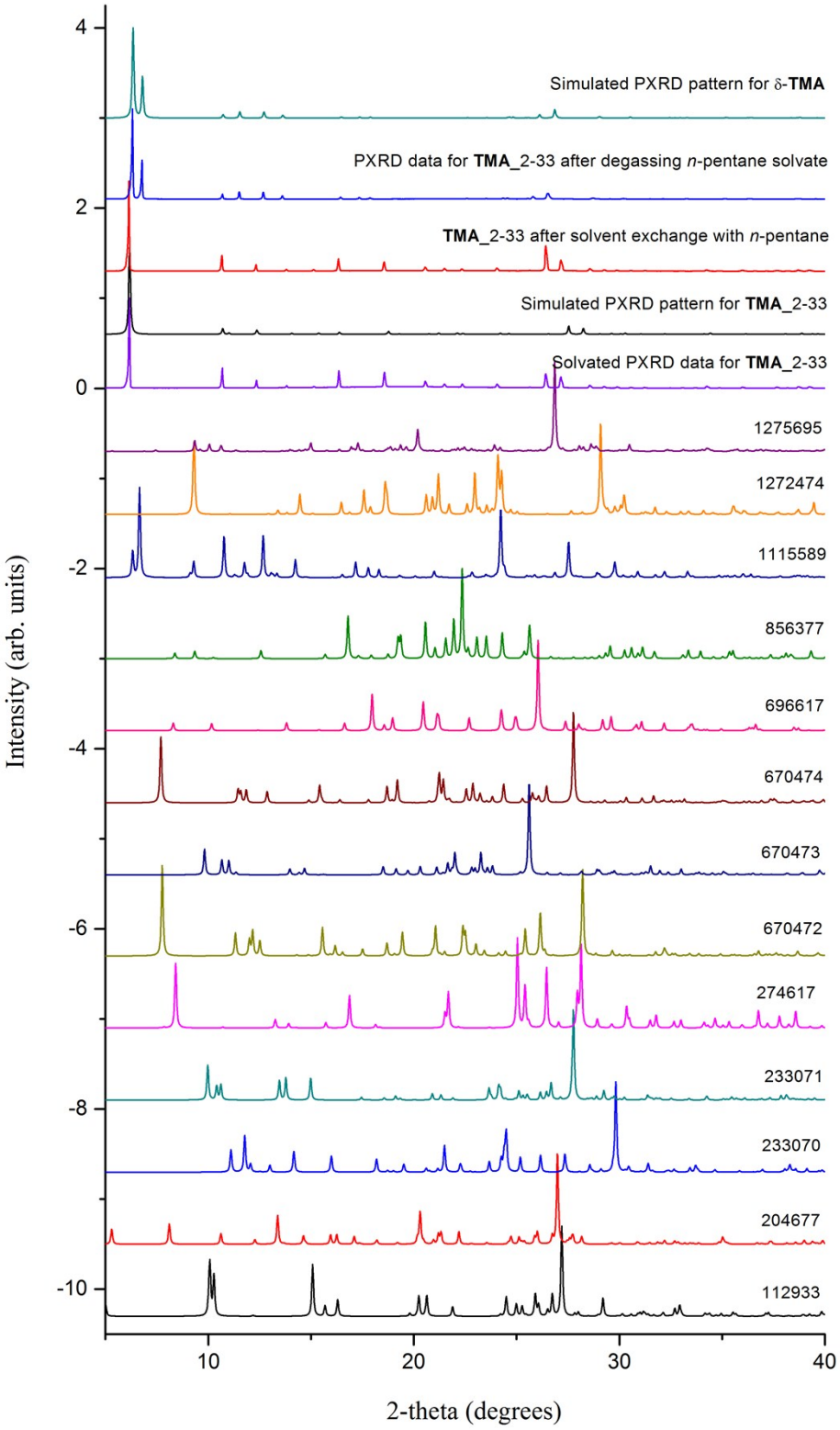

Figure S6. Solvated PXRD data for **TMA**_2-33, collected as a suspension in a glass capillary. The PXRD data for this structure is shown below the following; the simulated PXRD pattern for this structure (black); after exchanging the crystallisation solvent with *n*-pentane (red); after degassing the *n*-pentane exchanged sample at room temperature for 2 hrs. (blue); and the simulated PXRD pattern of the predicted low-density **TMA** phase, **1** (δ-**TMA**, olive green, top). The simulated PXRD patterns for the known **TMA** structure are shown below the experimental data.

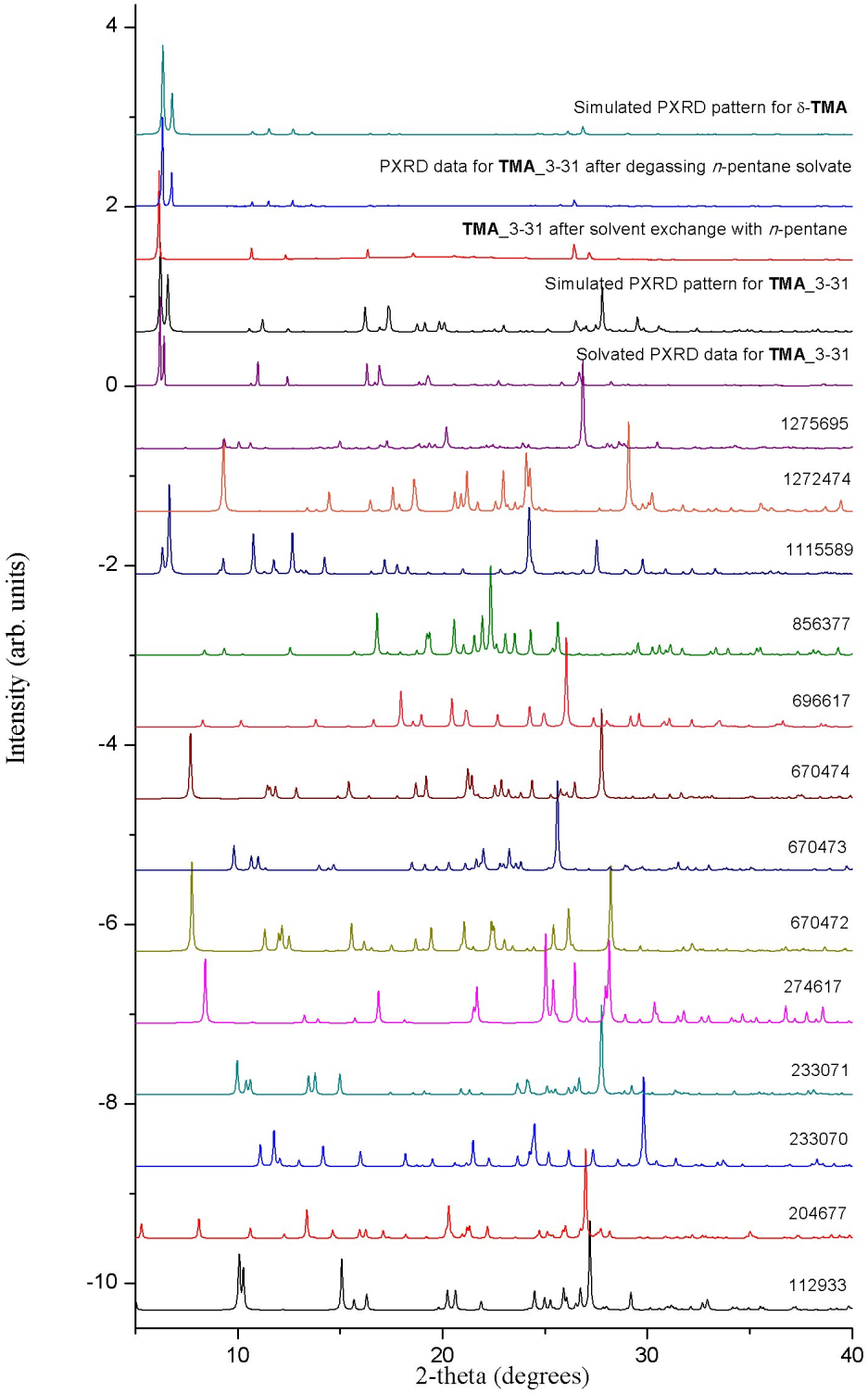

Figure S7. Solvated PXRD data for **TMA**_3-31, collected as a suspension in a glass capillary. The PXRD data for this structure is shown below the following; the simulated PXRD pattern for this structure (black); after exchanging the crystallisation solvent with *n*-pentane (red); after degassing the *n*-pentane exchanged sample at room temperature for 2 hrs. (blue); and the simulated PXRD pattern of the predicted low-density **TMA** phase, **1** (δ-**TMA**, olive green, top). The simulated PXRD patterns for the known **TMA** structure are shown below the experimental data.

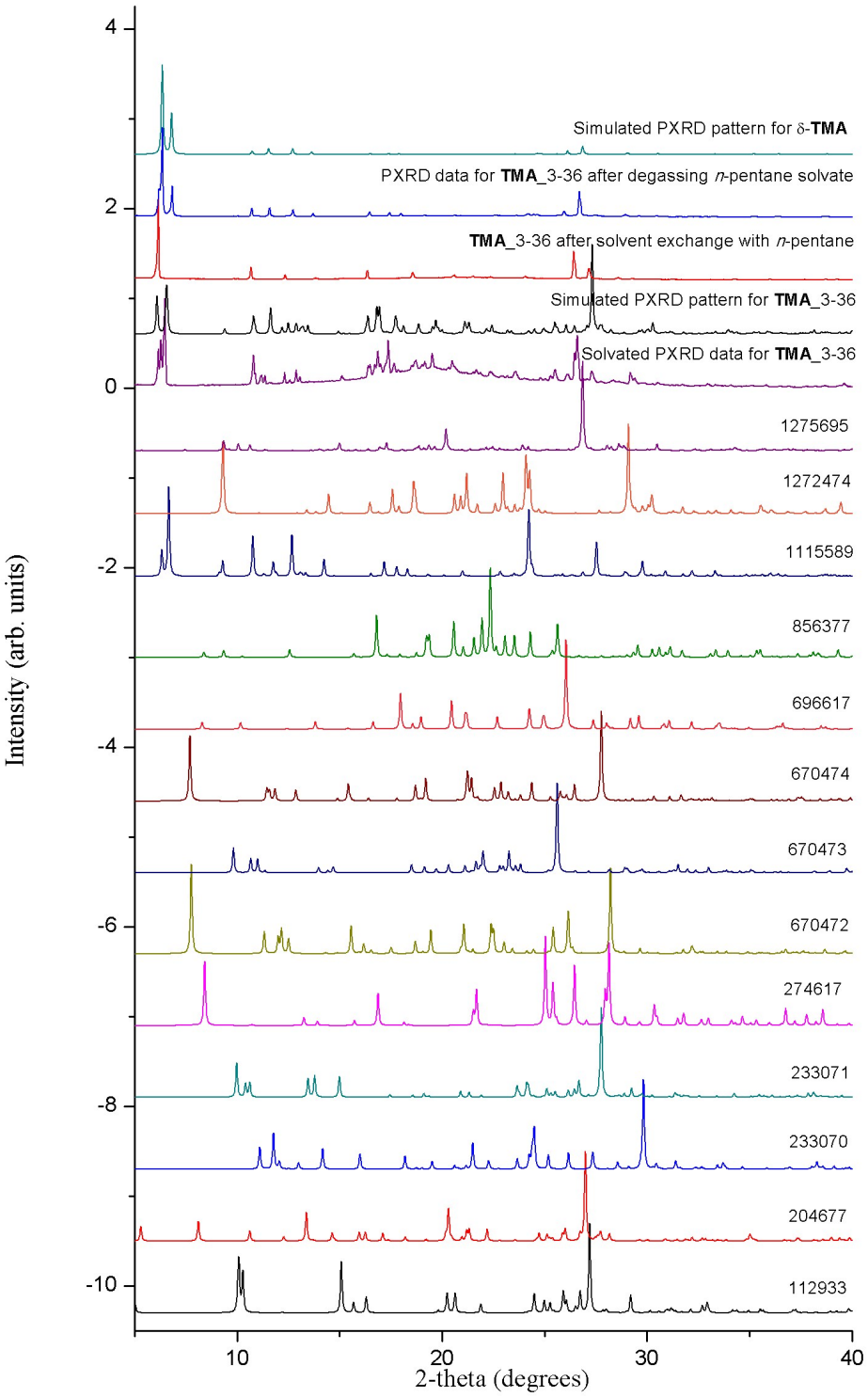

Figure S8. Solvated PXRD data for **TMA**_3-36, collected as a suspension in a glass capillary. The PXRD data for this structure is shown below the following; the simulated PXRD pattern for this structure (black); after exchanging the crystallisation solvent with *n*-pentane (red); after degassing the *n*-pentane exchanged sample at room temperature for 2 hrs. (blue); and the simulated PXRD pattern of the predicted low-density **TMA** phase, **1** (δ-**TMA**, olive green, top). The simulated PXRD patterns for the known **TMA** structure are shown below the experimental data.

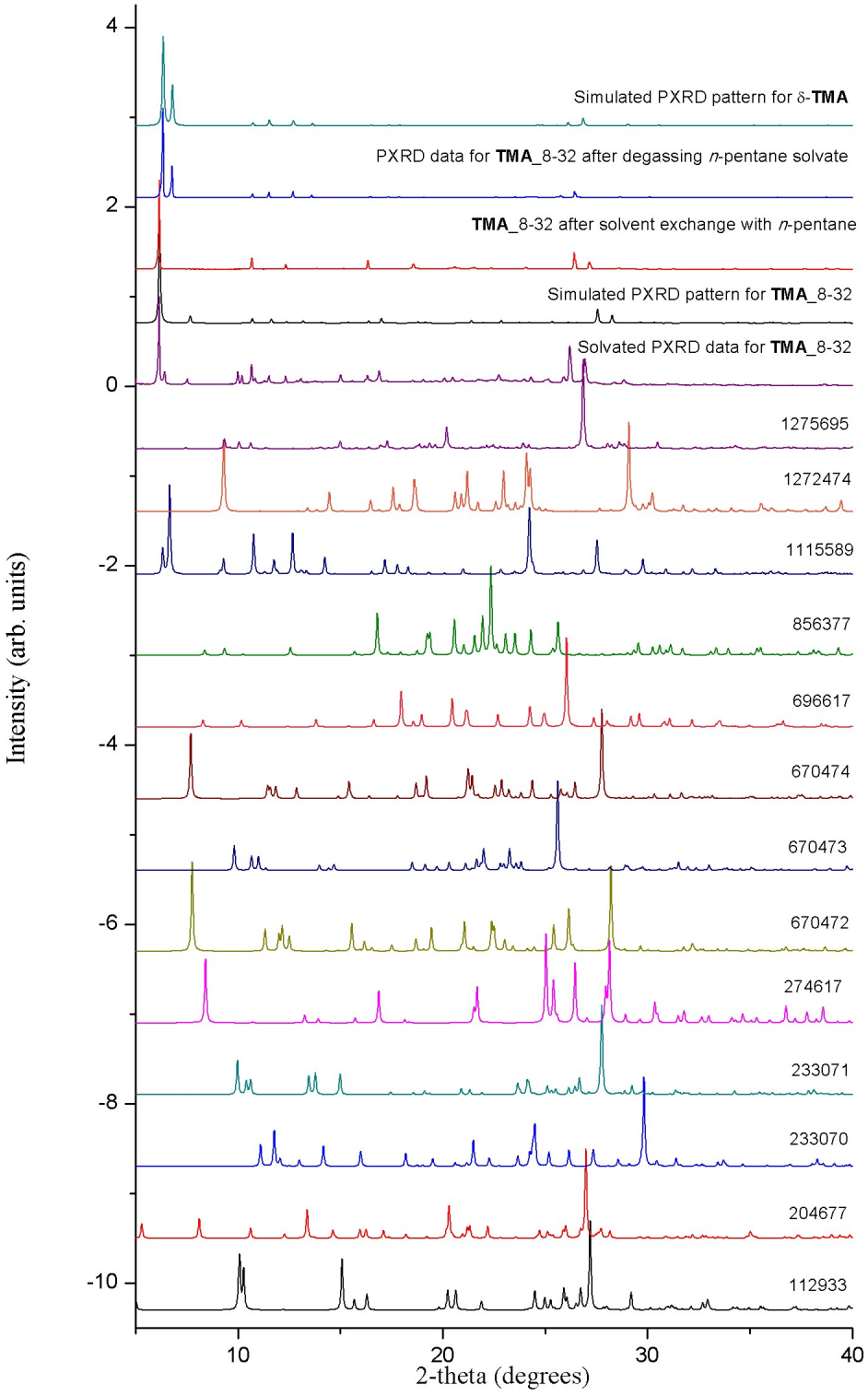

Figure S9. Solvated PXRD data for **TMA**_8-32, collected as a suspension in a glass capillary. The PXRD data for this structure is shown below the following; the simulated PXRD pattern for this structure (black); after exchanging the crystallisation solvent with *n*-pentane (red); after degassing the *n*-pentane exchanged sample at room temperature for 2 hrs. (blue); and the simulated PXRD pattern of the predicted low-density **TMA** phase, **1** (δ-**TMA**, olive green, top). The simulated PXRD patterns for the known **TMA** structure are shown below the experimental data.

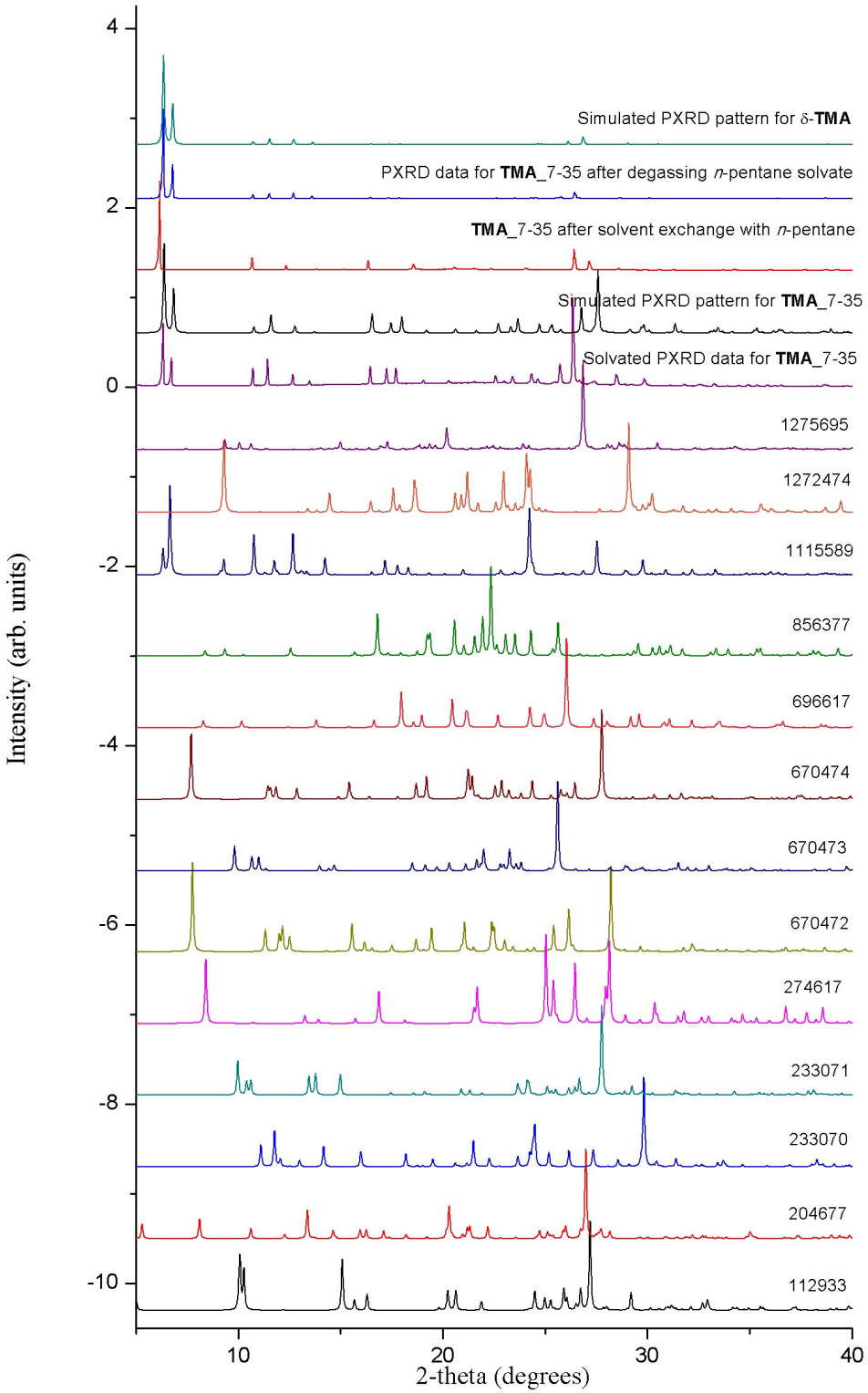

Figure S10. Solvated PXRD data for **TMA**_7-35, collected as a suspension in a glass capillary. The PXRD data for this structure is shown below the following; the simulated PXRD pattern for this structure (black); after exchanging the crystallisation solvent with *n*-pentane (red); after degassing the *n*-pentane exchanged sample at room temperature for 2 hrs. (blue); and the simulated PXRD pattern of the predicted low-density **TMA** phase, **1** (δ-**TMA**, olive green, top). The simulated PXRD patterns for the known **TMA** structure are shown below the experimental data.

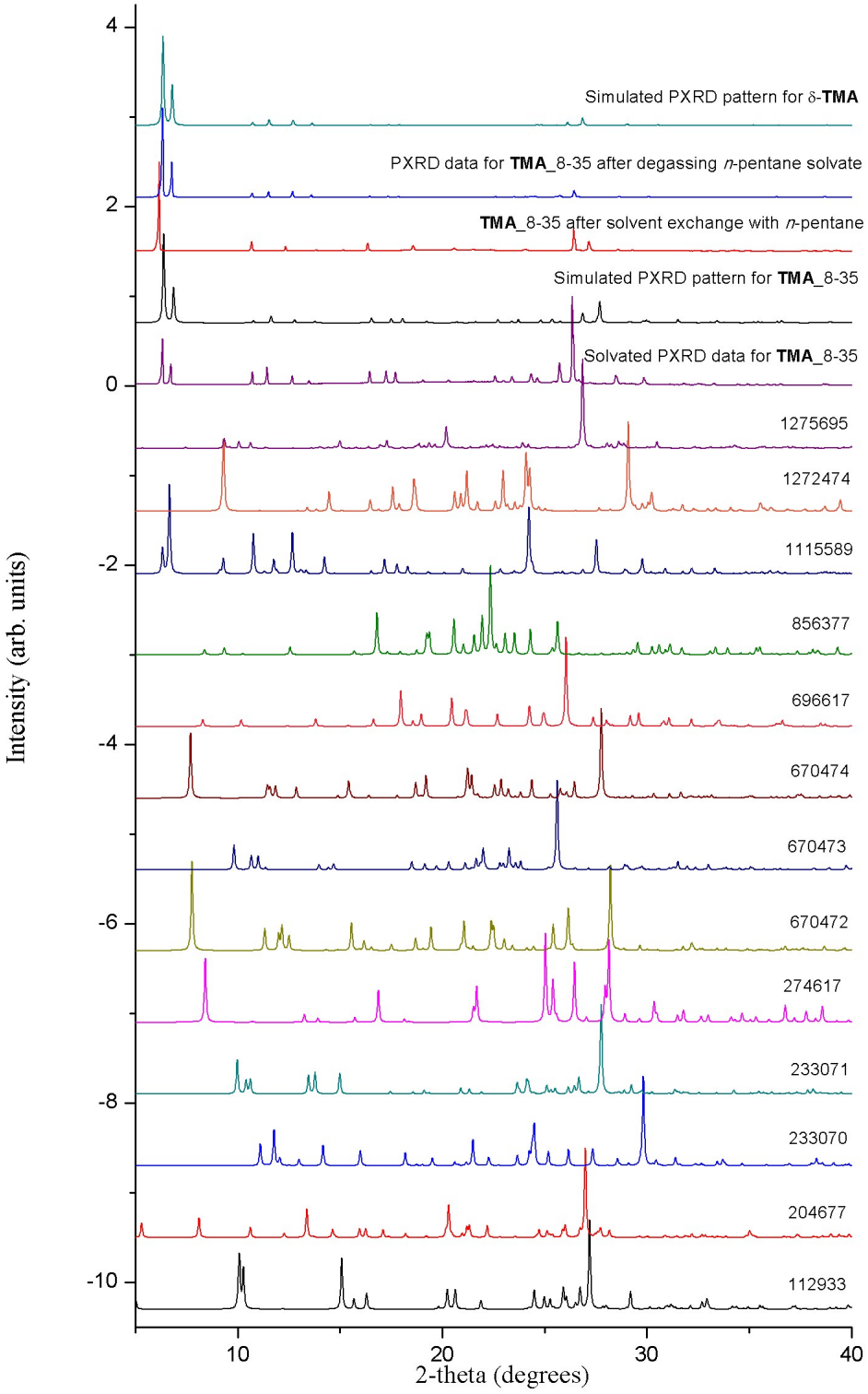

Figure S11. Solvated PXRD data for **TMA**_8-35, collected as a suspension in a glass capillary. The PXRD data for this structure is shown below the following; the simulated PXRD pattern for this structure (black); after exchanging the crystallisation solvent with *n*-pentane (red); after degassing the *n*-pentane exchanged sample at room temperature for 2 hrs. (blue); and the simulated PXRD pattern of the predicted low-density **TMA** phase, **1** (δ-**TMA**, olive green, top). The simulated PXRD patterns for the known **TMA** structure are shown below the experimental data.

Scale up, solvent exchange and activation of TMA_2-33

TMA (150 mg, 0.7 mmol) was dissolved in THF (10 mL) at room temperature. *n*-butylbenzene (10 mL) was slowly layered on top of the THF solution through a needle and the solvents were allowed to evaporate at room temperature. After 3 days, crystal had formed in the glass vial and the residual solvent was removed via syringe. *n*-Pentane (20 mL) was added to fully immerse the crystals and the *n*-pentane solvent was exchanged every 12 hours for 5 days. ^{1}H NMR was used to determine the composition of the solvent molecules in the pores in the crystal structure.

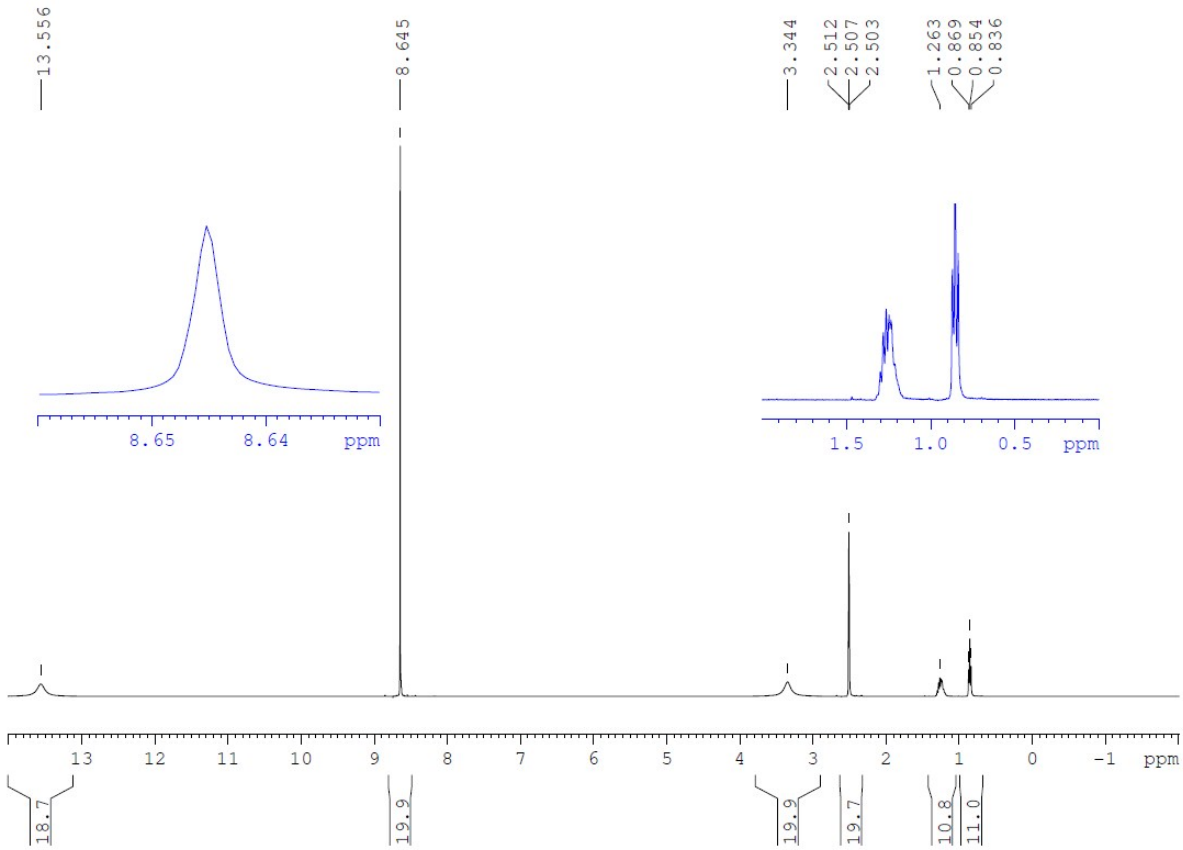

Figure S12. ^{1}H NMR spectrum (400 MHz, DMSO-d_6) of δ-**TMA**. The NMR signal was assigned accordingly, **TMA** [δ (ppm.) 8.64 (s, 3H, PhenylH) and 13.5 (s, 3H, COOH)], and pentane [δ (ppm.) 1.26 (-CH_2) and 0.85 (-CH_3)]. The signals at 2.50 and 3.34 ppm. are DMSO and H_2O, respectively.

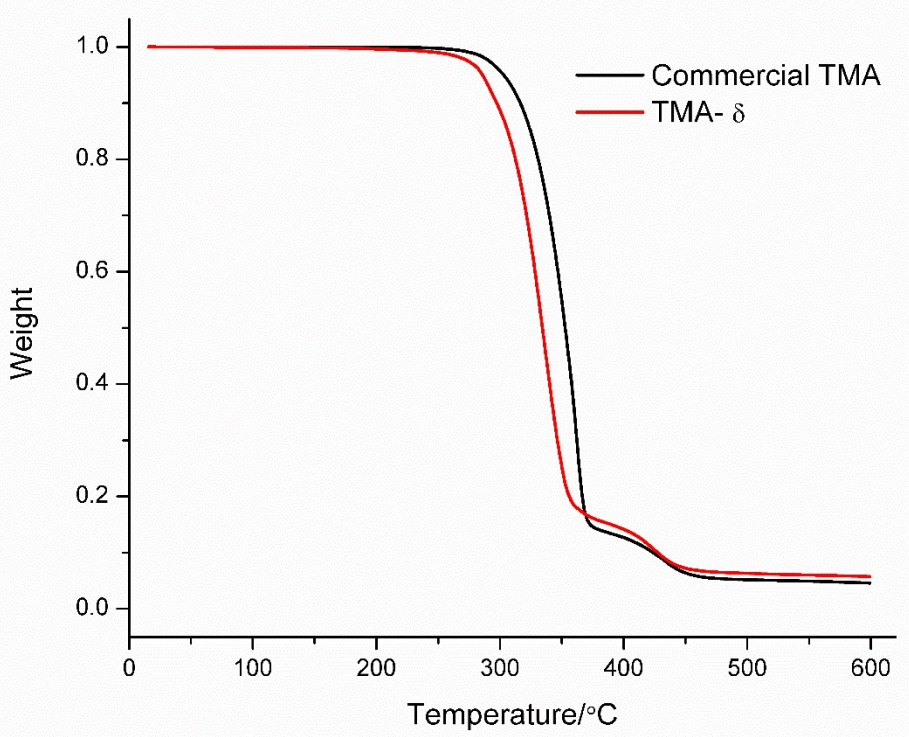

Figure S13. TGA plot of δ-**TMA**, recorded under a dry nitrogen gas flow after degassing the *n*-pentane exchanged crystals at room temperature for 1 h under dynamic vacuum (red). The TGA trace for commercially sourced **TMA** is shown in black.

Table S8. Single crystal X-ray refinement details for **TMA-δ**.

	TMA-δ (200K)	**TMA-δ** (350K)
Space Group	*C*2/*m*	*C*2/*m*
Wavelength [Å]	Mo-Kα	Mo-Kα
Collection Temperature	200 K	350 K
Formula	$C_9H_6O_6$	$C_9H_6O_6$
Mr	210.14	210.14
Crystal Size (mm)	0.15 x 0.14 x 0.09	0.15 x 0.14 x 0.09
Crystal System	Monoclinic	Monoclinic
a [Å]	26.075(2)	26.240(5)
b [Å]	16.4837(12)	16.529(3)
c [Å]	3.6749(3)	3.7452(7)
V [Å^3]	1573.3(2)	1614.6(5)
α [°]		
β [°]	95.076(2)	96.283(6)
γ [°]		
Z	4	4
D_{calcd} [g cm^{-3}]	0.887	0.864
μ [mm^{-1}]	0.077	0.075
F(000)	432	432
2θ range [°]	4.94 – 53.37	4.93 – 52.94
Reflections collected	8938	9783
Independent reflections, R_{int}	1723, 0.0430	1731, 0.379
Obs. Data [$I > 2\sigma$]	1324	1183
Data / restraints / parameters	1723 / 0 / 75	1731 / 0 / 75
Final R1 values ($I > 2\sigma(I)$)	0.0406	0.0423
Final R1 values (all data)	0.0547	0.0622
Final wR(F^2) values (all data)	0.1206	0.1342
Goodness-of-fit on F^2	1.042	1.020
Largest difference peak and hole [e.A^{-3}]	0.209 / -0.230	0.148 / -0.158
CCDC	1915307	1915306

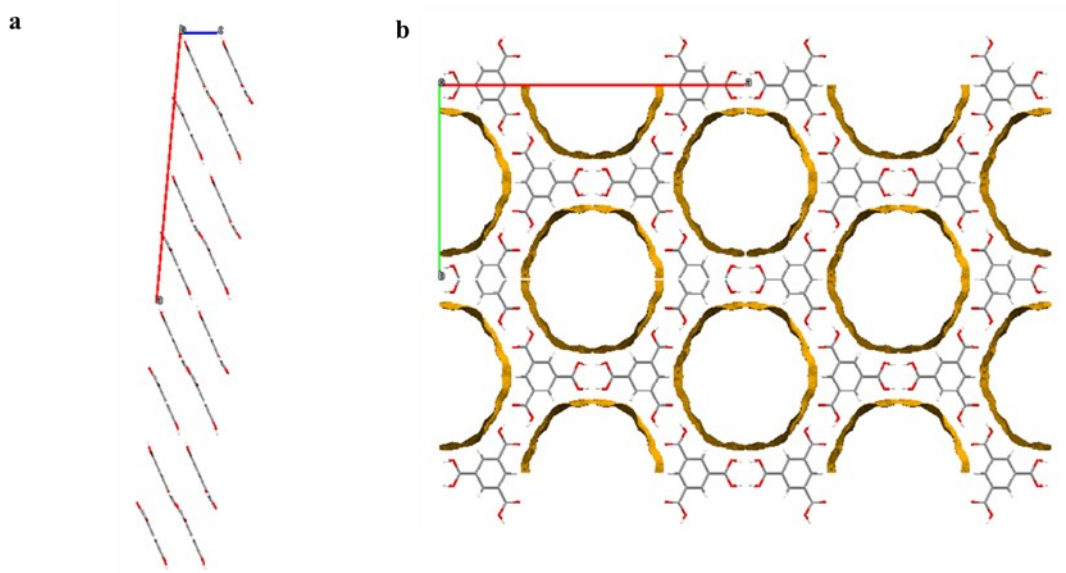

Figure S14. (**a**) Extended crystal packing from the single crystal structure of δ-**TMA** recorded at 200K; shown along the crystallographic *b* (**a**) and *c* (**b**) axes. In the structure, the trimesic acid molecule are stacked at a distance of 3.68 Å. The empty, solvent-accessible space (1.4 Å probe radius, 0.1 Å grid spacing) makes up approximately 50.6 % of the unit cell volume [796.51 Å^3 (V_{cell} = 1573.3 Å^3)].

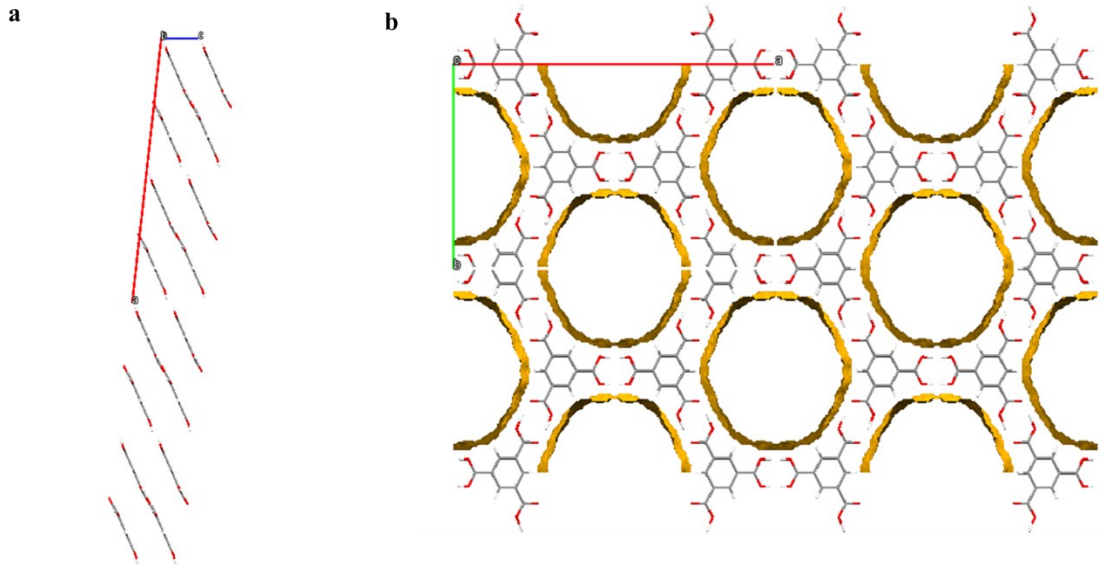

Figure S15. (**a**) Extended crystal packing from the single crystal structure of δ-**TMA** recorded at 350K; shown along the crystallographic *b* (**a**) and *c* (**b**) axes. In the structure, the trimesic acid molecules are stacked at a distance of 3.75 Å.

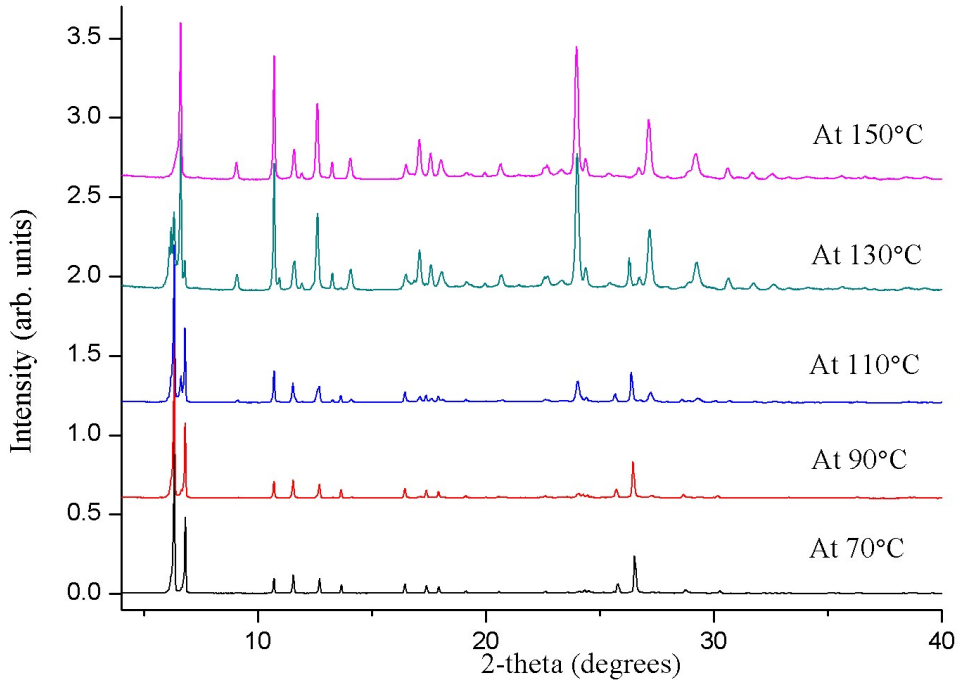

Figure S16. Variable temperature PXRD pattern for activated δ-**TMA**, recorded over the temperature range 70-150 °C. At 110 °C we observed the δ-**TMA** structure beginning to transform to the α-polymorph.

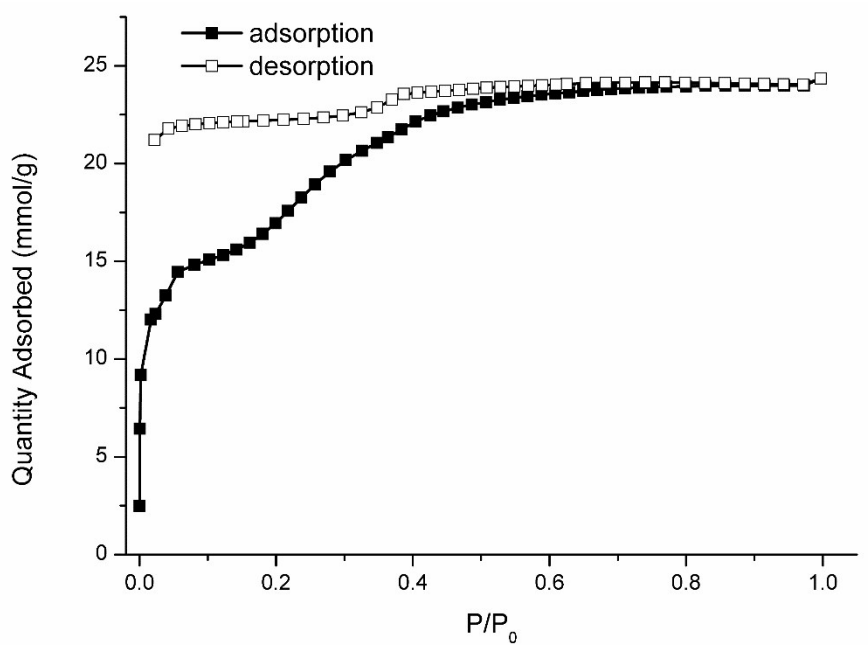

Figure S17. N_2 gas sorption isotherm for δ-**TMA** recorded at 77.3 K.

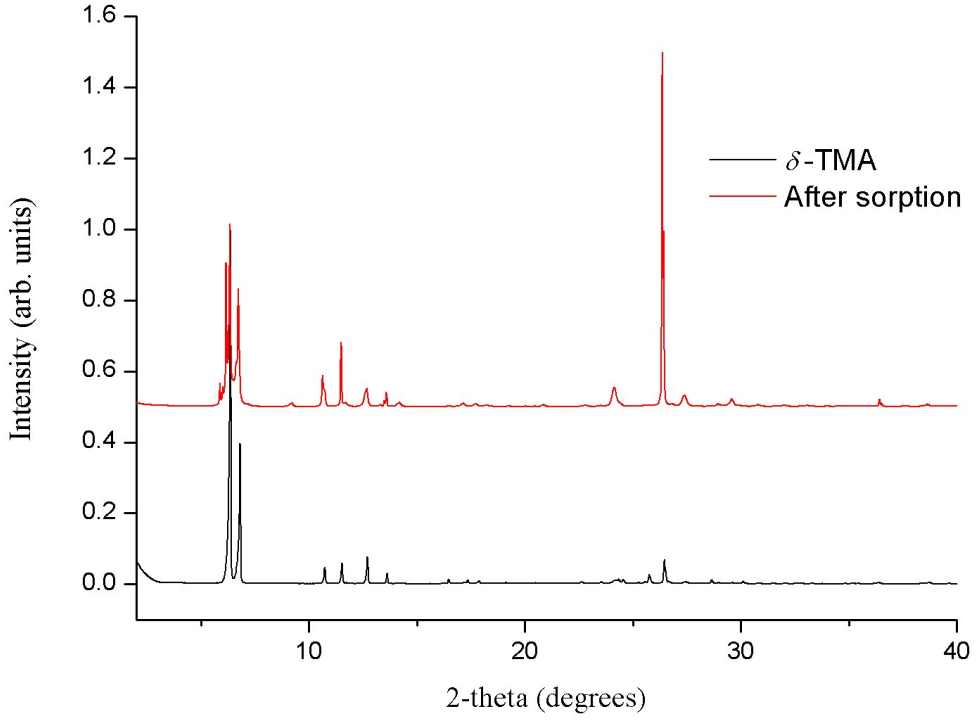

Figure S18. PXRD patterns of δ-**TMA** recorded before and after N_2 adsorption and desorption cycles. PXRD data collected post gas sorption analysis indicated that there was some of the α-**TMA** polymorph present in the sample.

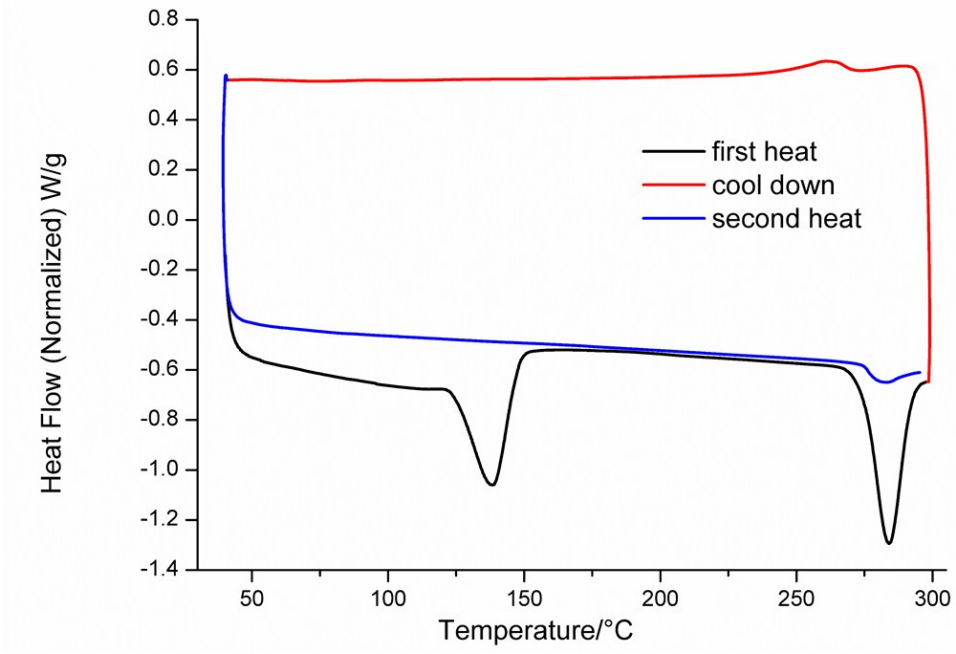

Figure S19. DSC trace for δ-**TMA**, recorded after activating the *n*-pentane solvated sample under vacuum at RT for 1 hour.

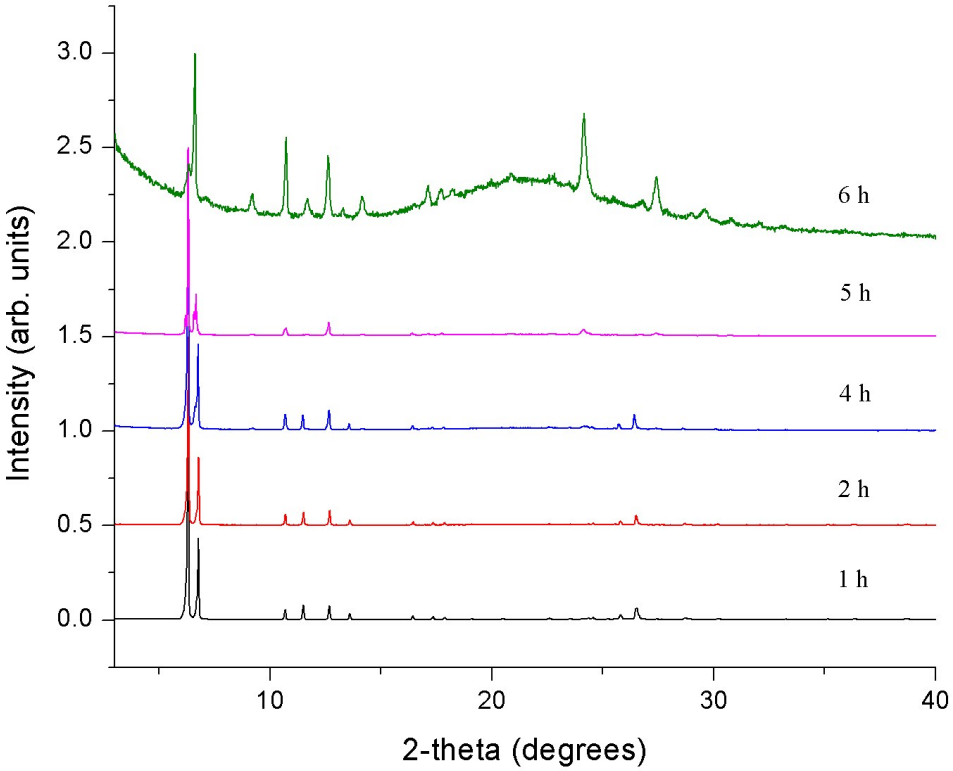

Figure S20. PXRD patterns for δ-**TMA**, recorded after degassing the sample under dynamic vacuum for 1-6 h, at room temperature.

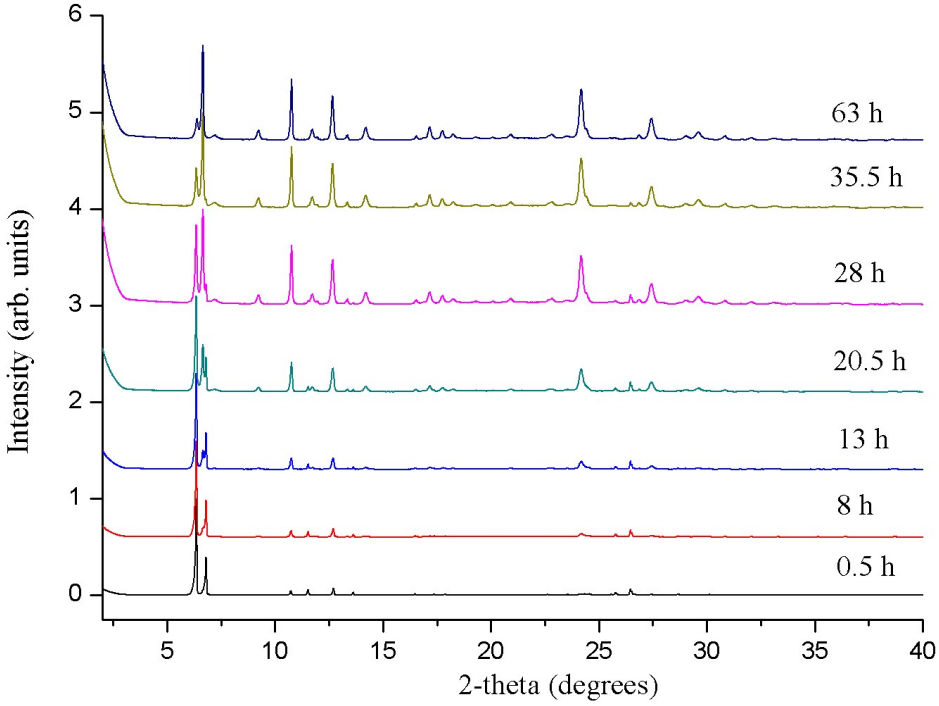

Figure S21. PXRD patterns for δ-**TMA**, recorded after standing the activated material in humid air at room temperature.

Table S9. Single crystal X-ray refinement details for solvated **ADTA** structures.

	ADTA_3-38	**ADTA_7-38**	**ADMA_2-2**
	3-fold	3-fold	4-fold
Crystallisation Solvent	EtOH/tetradecane	Dioxane/tetradecane	THF
Space Group	*Fddd*	$I4_1/amd$	$I4_1/a$
Wavelength [Å]	Mo-Kα	Mo-Kα	Mo-Kα
Collection Temperature	200 K	200 K	100 K
Formula	$C_{14}H_{16}O_8 \cdot 0.43(C_{14}H_{30})$	$C_{14}H_{16}O_8 \cdot 0.43(C_{14}H_{30})$	$C_{14}H_{16}O_8 \cdot 0.25(C_4H_8O)$
Mr	397.29	397.50	330.29
Crystal Size (mm)	0.11 x 0.08 x 0.05	0.15 x 0.15 x 0.13	0.12 x 0.12 x 0.11
Crystal System	Orthorhombic	Tetragonal	Tetragonal
a [Å]	7.3713(11)	16.429(3)	16.4008(15)
b [Å]	22.951(4)		
c [Å]	23.585(4)	7.3580(12)	22.397(2)
V [Å^3]	3990.0(11)	1986.0(7)	6024.5(13)
Z	8	4	16
D_{calcd} [g cm^{-3}]	1.323	1.329	1.457
μ [mm^{-1}]	0.102	0.102	0.120
F(000)	1703	852	2784
2θ range [°]	4.95 – 52.75	4.96 – 52.75	4.97 – 58.27
Reflections collected	8009	7390	40618
Independent reflections, R_{int}	1028, 0.0818	554, 0.0598	4055, 0.0493
Obs. Data [$I > 2\sigma$]	628	407	4055
Data / restraints / parameters	1028 / 3 / 67	554 / 1 / 47	4055 / 14 / 238
Final R1 values ($I > 2\sigma(I)$)	0.0634	0.0650	0.0549
Final R1 values (all data)	0.1034	0.0842	0.0686
Final wR(F^2) values (all data)	0.2143	0.1993	0.1635
Goodness-of-fit on F^2	1.039	1.135	1.053
Largest difference peak and hole [e.A^{-3}]	0.332/-0.260	0.241 / -0.242	0.485 / -0.271
CCDC	1915300	1915302	1915301

Table S10. Single crystal X-ray refinement details for solvated 2-fold **ADTA** structures.

	ADTA_2-34	**ADTA_2-27[a]**	**ADTA_2-35[b]**
	2-fold	2-fold	2-fold
Crystallisation Solvent	THF/1,3-dimethoxybenzene	THF/*ortho*-xylene	THF/1,3-dimethoxybenzene
Space Group	$I4_1/a$	$Pn\bar{3}$	$P4_2/nnm$
Wavelength [Å]	Mo-Kα	Mo-Kα	Mo-Kα
Collection Temperature	100 K	100 K	200 K
Formula	$2(C_{14}H_{16}O_8)\cdot4(C_8H_{10}O_2)$	$C_{14}H_{20}O_8\cdot8.75(O)$	$C_{14}H_{20}O_8\cdot17.5(O)$
Mr	1177.17	456.30	596.30
Crystal Size (mm)	0.11 x 0.09 x 0.07	0.40 x 0.39 x 0.38	0.14 x 0.11 x 0.11
Crystal System	Tetragonal	Cubic	Tetragonal
a [Å]	16.2380(2)	14.4074(5)	11.4331(8)
b [Å]			
c [Å]	22.3825(3)		11.4312(8)
V [Å^3]	5901.65(17)	1484.4(2)	1494.2(2)
Z	4	2	2
D_{calcd} [g cm^{-3}]	1.325	1.021	1.325
μ [mm^{-1}]	0.103	0.097	0.134
F(000)	2496	476	616
2θ range [°]	5.02 – 52.72	3.57 – 60.94	3.56 – 52.72
Reflections collected	45910	15739	17215
Independent reflections, R_{int}	3006, 0.0789	761, 0.0579	829, 0.0453
Obs. Data [$I > 2\sigma$]	2383	656	682
Data / restraints / parameters	3006 / 0 / 195	761 / 36 / 76	829 / 6 / 98
Final R1 values ($I > 2\sigma(I)$)	0.0511	0.0859	0.0760
Final R1 values (all data)	0.0639	0.0928	0.0860
Final wR(F^2) values (all data)	0.1421	0.2255	0.2009
Goodness-of-fit on F^2	1.064	1.196	1.142
Largest difference peak and hole [e.A^{-3}]	0.330 / -0.250	0.338 / -0.420	0.177 / -0.398
CCDC	1915303	1915299	1915312

[a] X-ray crystal structure refined with the TWINLAW [$\bar{1}$00 001 010] and BASF refined to 0.494. [b] X-ray crystal structure refined with the TWINLAW [$\bar{1}$00 001 010] and BASF refined to 0.532.

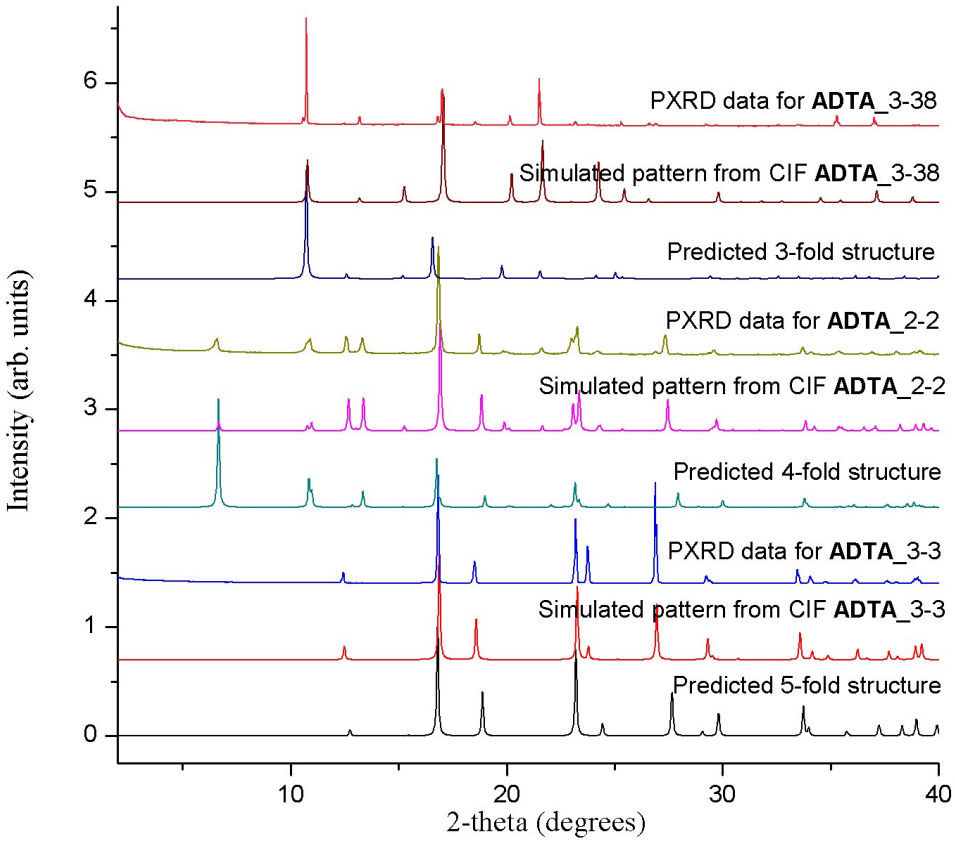

Figure S22. Experimental PXRD data from the HT crystallisation screen for **ADTA**_3-38, **ADTA**_2-2, and **ADTA**_3-3 *vs.* the simulated PXRD patterns for the predicted 3-, 4-, and 5-fold **ADTA** structures, and the simulated PXRD patterns for single crystal structures **ADTA**_3-38 (3-fold), **ADTA**_2-2 (4-fold), and **ADTA**_3-3 (5-fold).

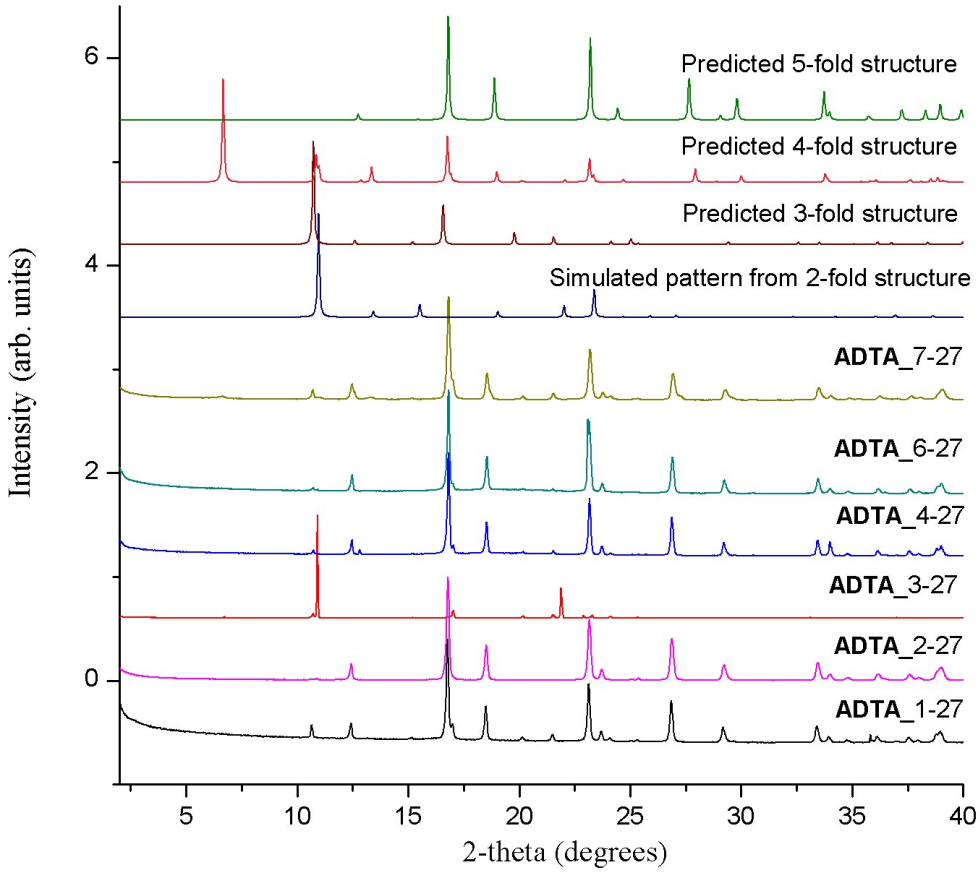

Figure S23. Experimental data from the **ADTA** crystallisation screen using the 6 'good solvents' (1: methanol, 2: THF, 3: ethanol, 4: 2-propanol, 6: 1-propanol, and 7: 1,4-dioxane) and the one bad solvent *o*-xylene (27). The unground samples were air dried on the PXRD plate before analysis. For comparison, the simulated PXRD patterns of the experimental 2-fold structure (**ADTA_2-27**) and the simulated PXRD patterns of the predicted 3-, 4-, and 5-fold structure are shown.

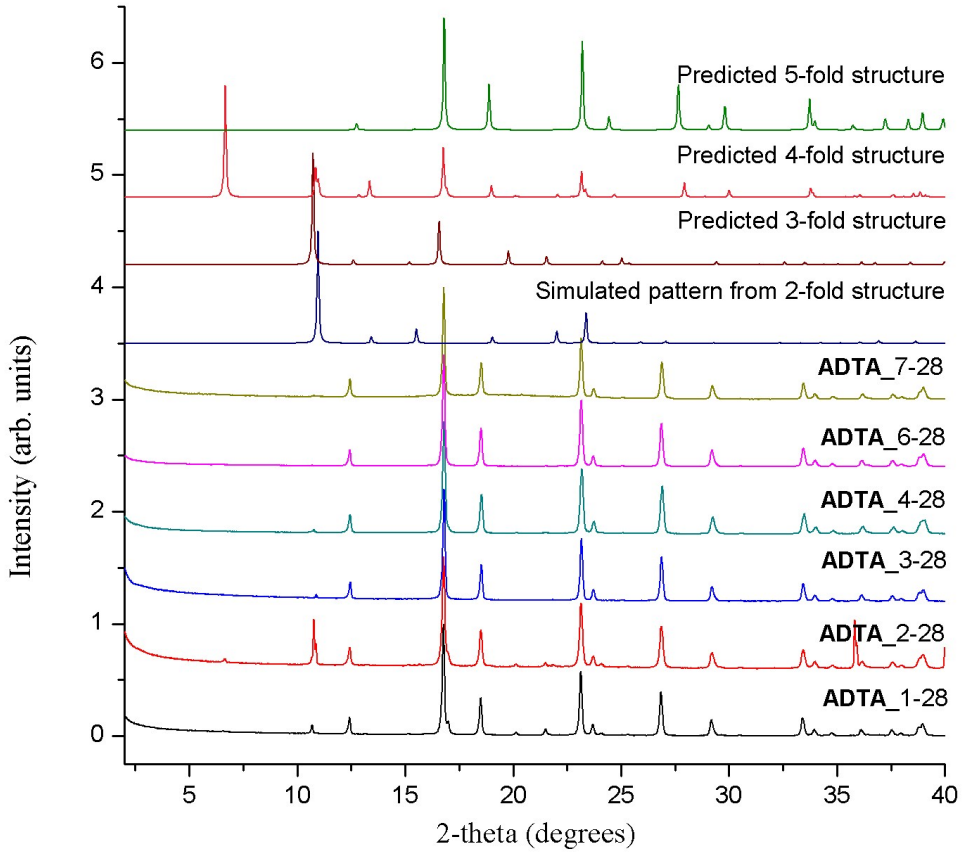

Figure S24. Experimental data from the **ADTA** crystallisation screen using the 6 'good solvents' (1: methanol, 2: THF, 3: ethanol, 4: 2-propanol, 6: 1-propanol, and 7: 1,4-dioxane) and the one bad solvent *m*-xylene (28). The unground samples were air dried on the PXRD plate before analysis. For comparison, the simulated PXRD patterns of the experimental 2-fold structure (**ADTA_2-27**) and the simulated PXRD patterns of the predicted 3-, 4-, and 5-fold structure are shown.

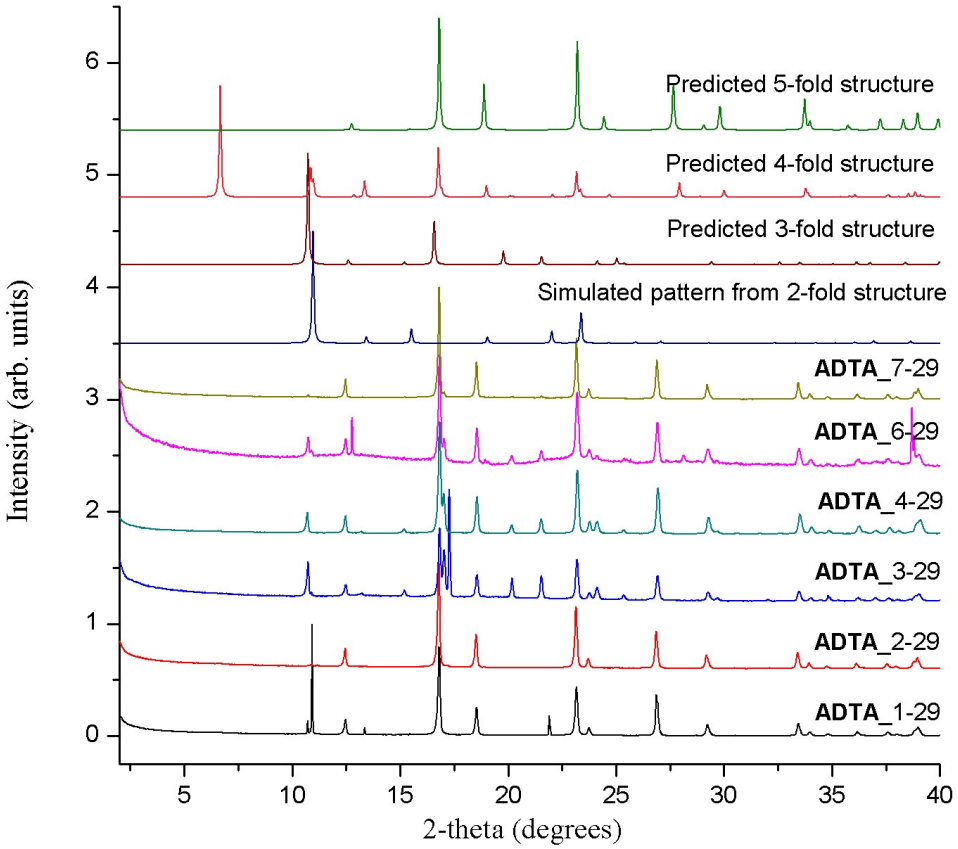

Figure S25. Experimental data from the **ADTA** crystallisation screen using the 6 'good solvents' (1: methanol, 2: THF, 3: ethanol, 4: 2-propanol, 6: 1-propanol, and 7: 1,4-dioxane) and the one bad solvent *p*-xylene (29). The unground samples were air dried on the PXRD plate before analysis. For comparison, the simulated PXRD patterns of the experimental 2-fold structure (**ADTA_2-27**) and the simulated PXRD patterns of the predicted 3-, 4-, and 5-fold structure are shown.

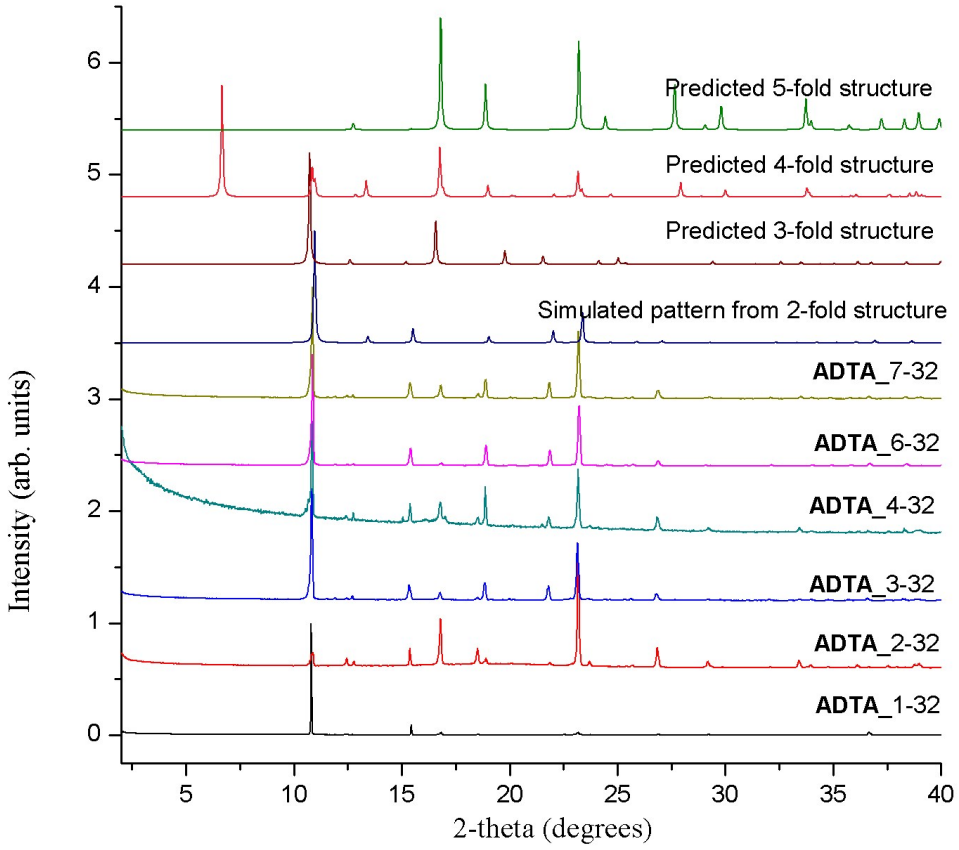

Figure S26. Experimental data from the **ADTA** crystallisation screen using the 6 'good solvents' (1: methanol, 2: THF, 3: ethanol, 4: 2-propanol, 6: 1-propanol, and 7: 1,4-dioxane) and the one bad solvent mesitylene (32). The unground samples were air dried on the PXRD plate before analysis. For comparison, the simulated PXRD patterns of the experimental 2-fold structure (**ADTA_2-27**) and the simulated PXRD patterns of the predicted 3-, 4-, and 5-fold structure are shown.

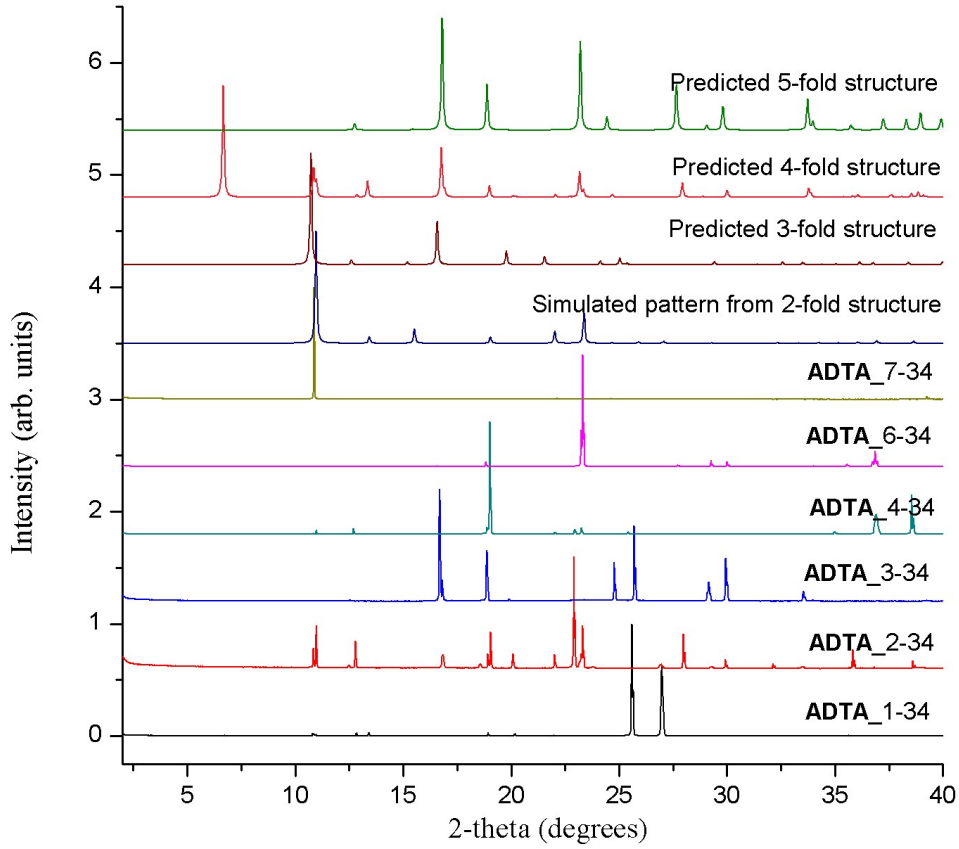

Figure S27. Experimental data from the **ADTA** crystallisation screen using the 6 'good solvents' (1: methanol, 2: THF, 3: ethanol, 4: 2-propanol, 6: 1-propanol, and 7: 1,4-dioxane) and the one bad solvent 1,2-dimethoxybenzene (34). The unground samples were air dried on the PXRD plate before analysis. For comparison, the simulated PXRD patterns of the experimental 2-fold structure (**ADTA_2-27**) and the simulated PXRD patterns of the predicted 3-, 4-, and 5-fold structure are shown.

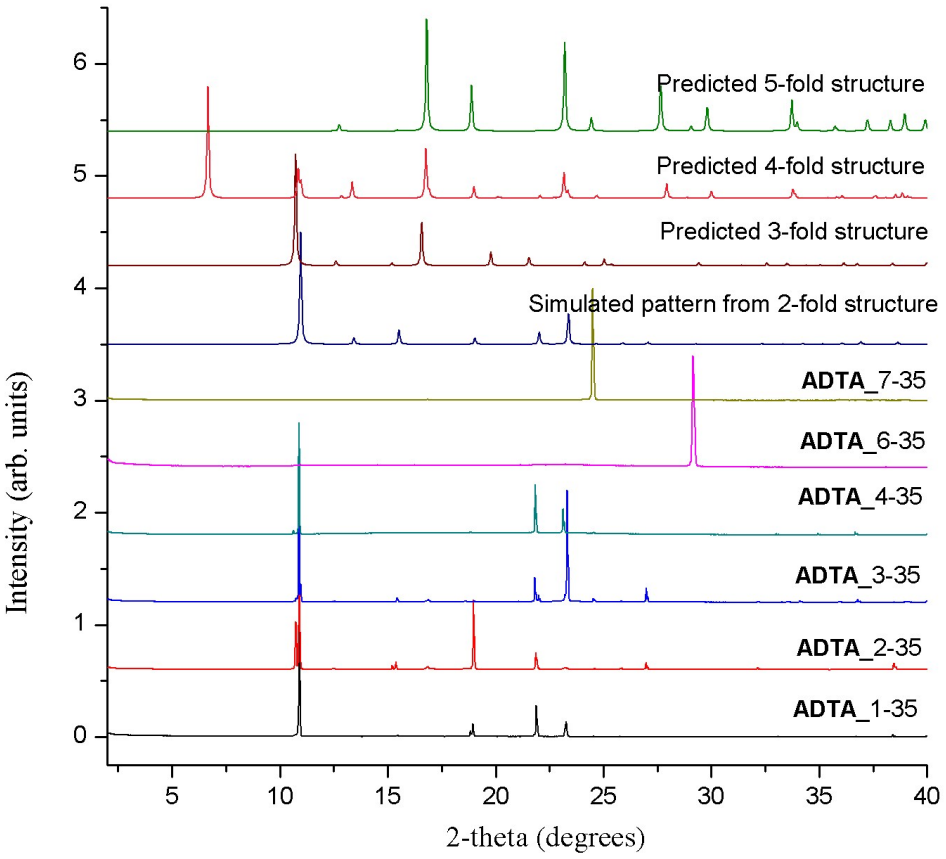

Figure S28. Experimental data from the **ADTA** crystallisation screen using the 6 'good solvents' (1: methanol, 2: THF, 3: ethanol, 4: 2-propanol, 6: 1-propanol, and 7: 1,4-dioxane) and the one bad solvent 1,3-dimethoxybenzene (35). The unground samples were air dried on the PXRD plate before analysis. For comparison, the simulated PXRD patterns of the experimental 2-fold structure (**ADTA_2-27**) and the simulated PXRD patterns of the predicted 3-, 4-, and 5-fold structure are shown.

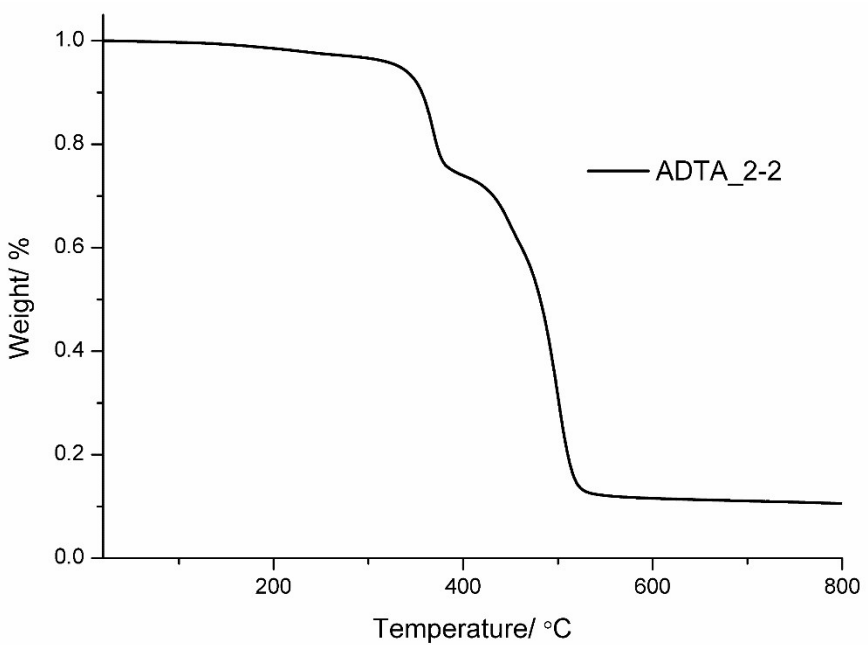

Figure S29. TGA plot for **ADTA**_2-2, recorded after degassing the sample at 100 °C for 10 hrs.

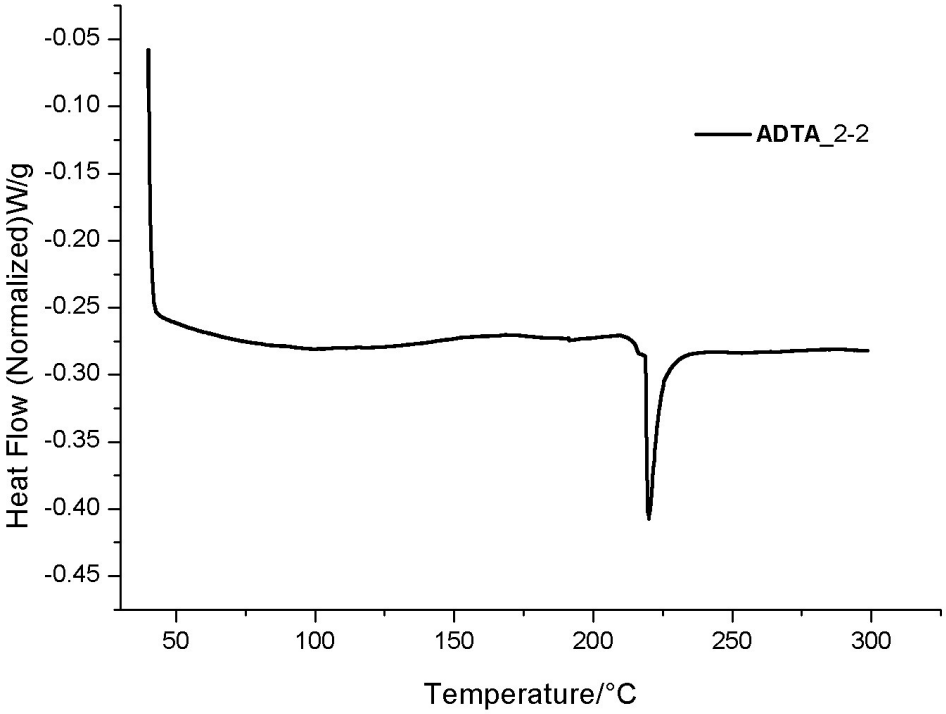

Figure S30. DSC plot of **ADTA**_2-2, recorded after degassing the sample at 100 °C for 10 hrs.

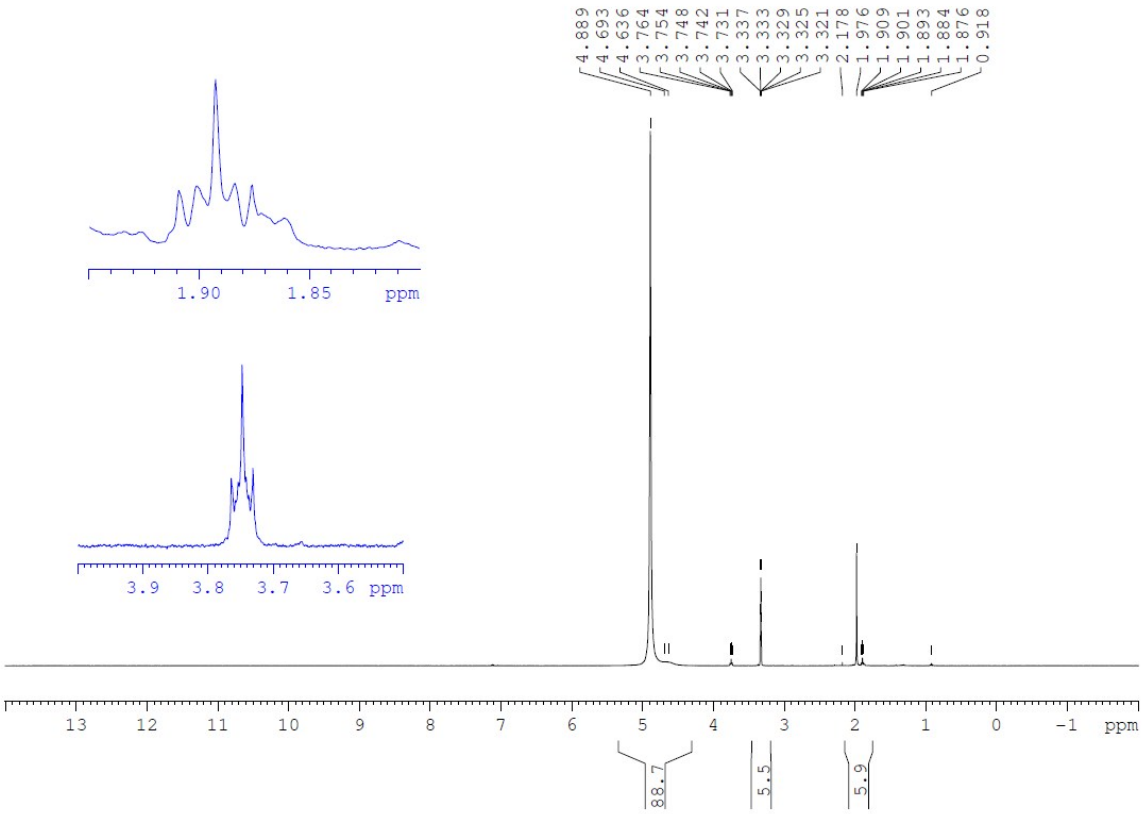

Figure S31. ^{1}H NMR spectrum (400 MHz, CD_3OD-d_4) of **ADTA**_2-2 after degassing the sample at 100 °C under vacuum. ADTA [δ (ppm.) 1.98 (s, -CH_2-)]. THF [δ (ppm.) 1.89 (m, O-CH_2-) and 3.74 (m, C-CH_2-C)]. The signals at 3.33 and 4.89 ppm. are CH_3OH and H_2O, respectively.

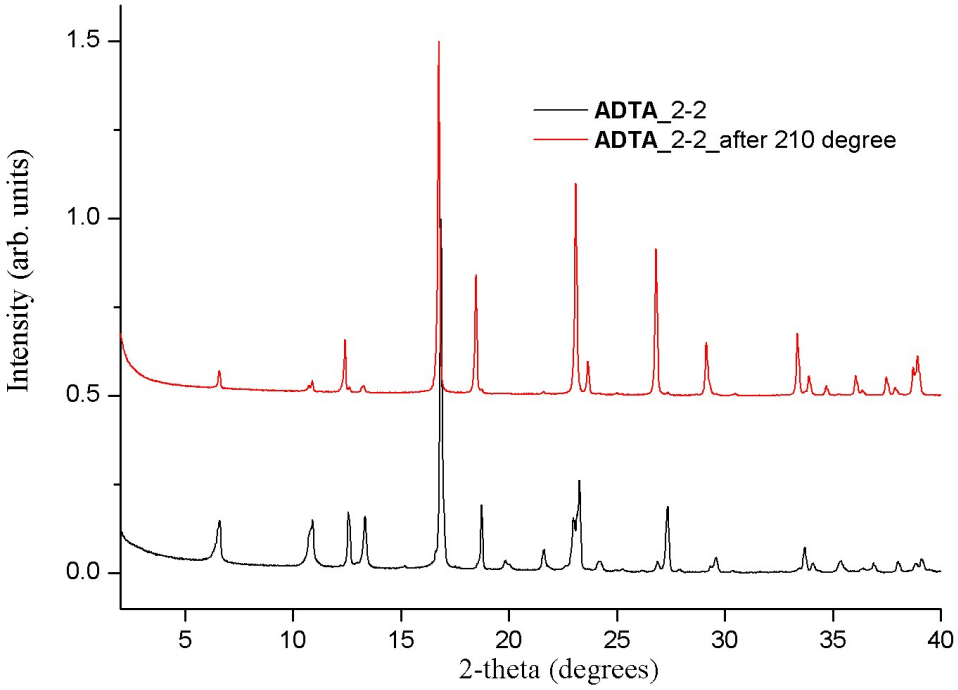

Figure S32. PXRD patterns for solvated **ADTA**_2-2 (black), and after heating **ADTA**_2-2 at 210 °C for 2.5 hrs. (red).

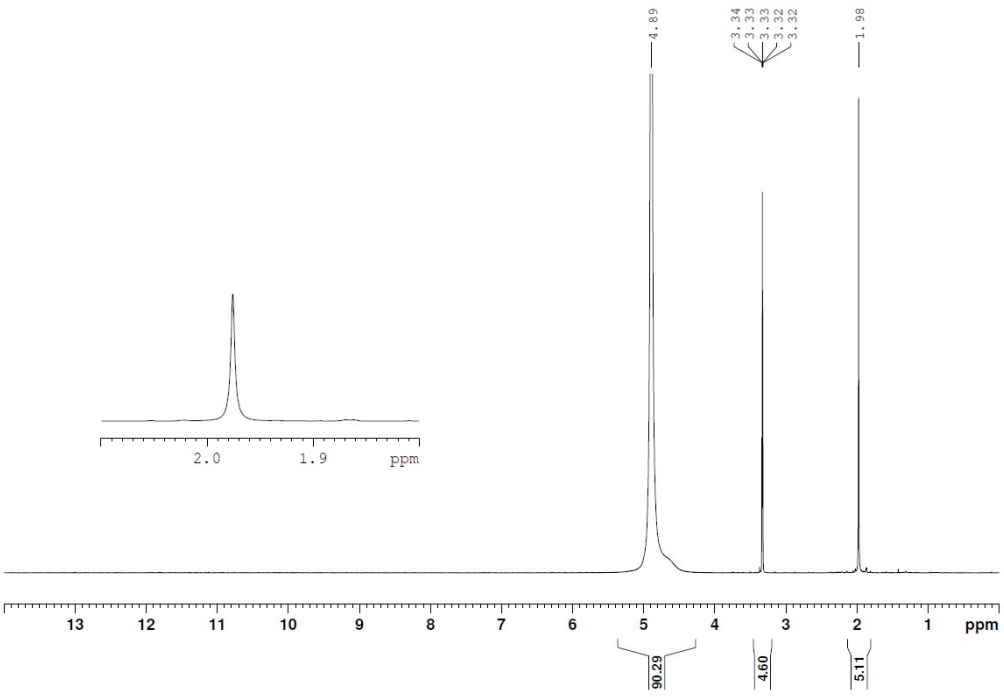

Figure S33. ^{1}H NMR spectrum (400 MHz, CD_3OD-d_4) of desolvated **ADTA**_2-2. **ADTA** [δ (ppm.) 1.98 (-CH_2)]. The signals at 3.33 and 4.89 ppm are CD_3OD and H_2O, respectively.

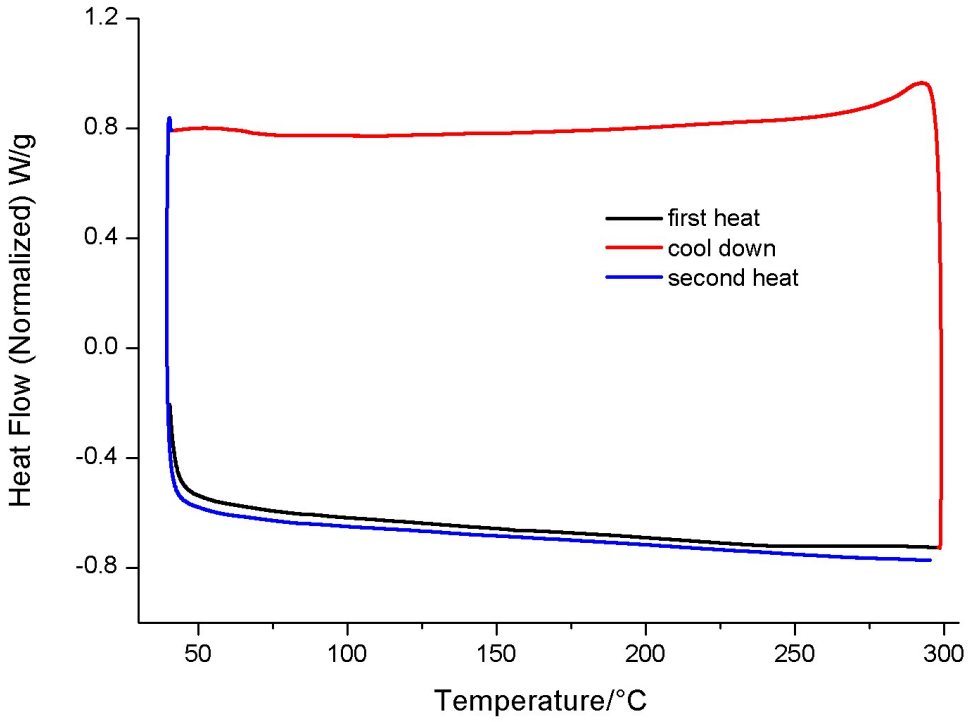

Figure S34. DSC plot of desolvated **ADTA**_2-2, recorded after previously heating crystalline material of the THF solvate at 210 °C for 2.5 hrs.

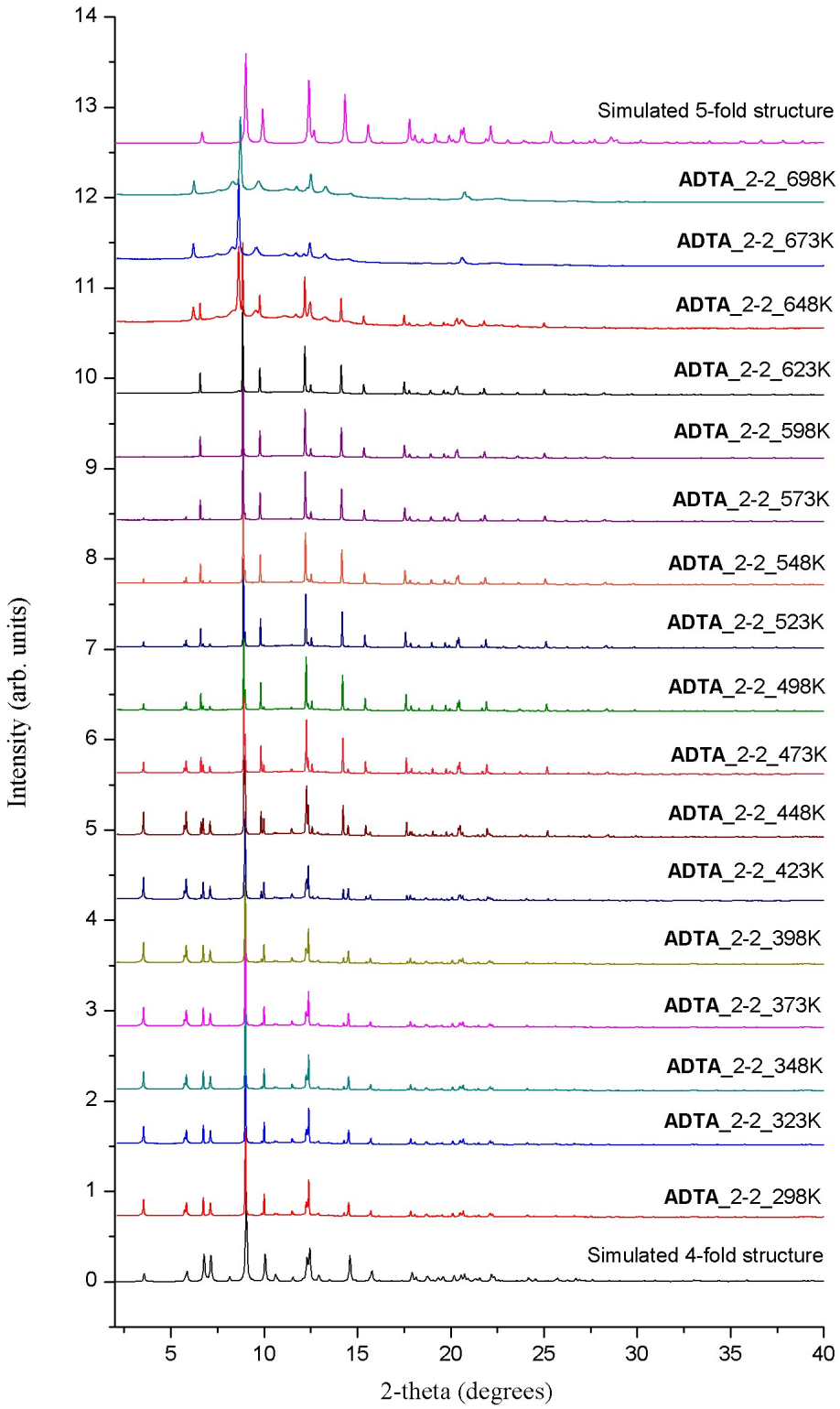

Figure S35. Variable temperature PXRD patterns for **ADTA**_2-2, recorded over the temperature range 298 K-698 K. (λ = 0.825186 Å). PXRD patterns were recorded every 25 K, after equilibrating the sample at each temperature for 15 minutes.

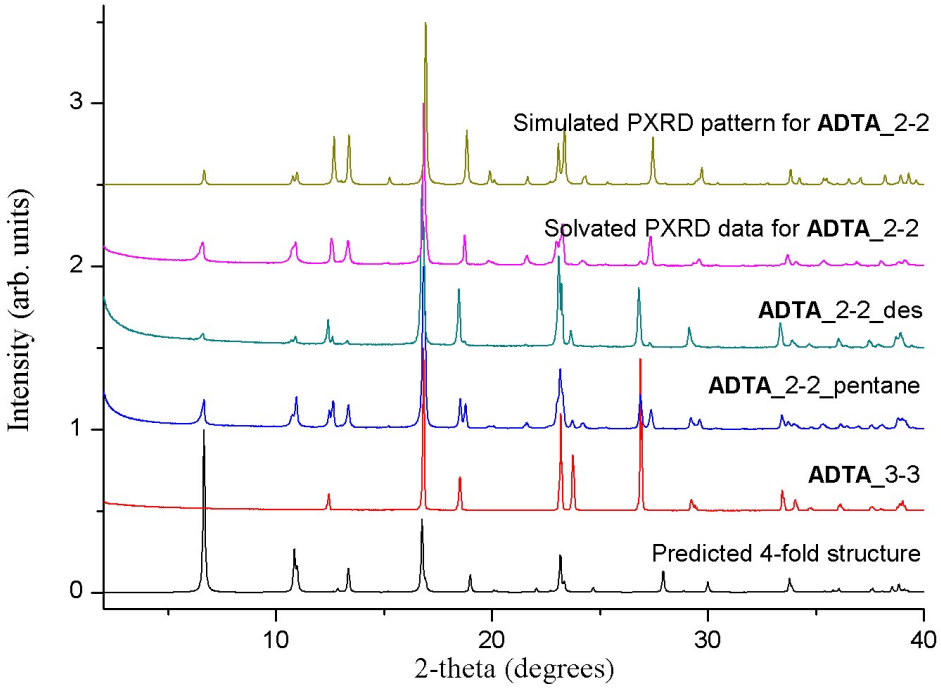

Figure S36. PXRD patterns recorded after activating the **ADTA**_2-2 THF solvate: Simulated PXRD pattern of the predicted 4-fold structure (black); simulated PXRD pattern of the experimental 5-fold structure **ADTA**_3-3 (red); experimental PXRD pattern for **ADTA**_2-2 that was recorded after attempting to exchanging the crystallisation solvent with *n*-pentane (blue); experimental PXRD pattern recorded after attempting to desolvate the THF solvate, **ADTA**_2-2, at 100 °C under dynamic vacuum (**ADTA**_2-2_des, cyan); experimental PXRD data for fully solvated **ADTA**_2-2 (pink), simulated PXRD pattern from the single crystal structure, **ADTA**_2-2 recorded at 100 K (green).

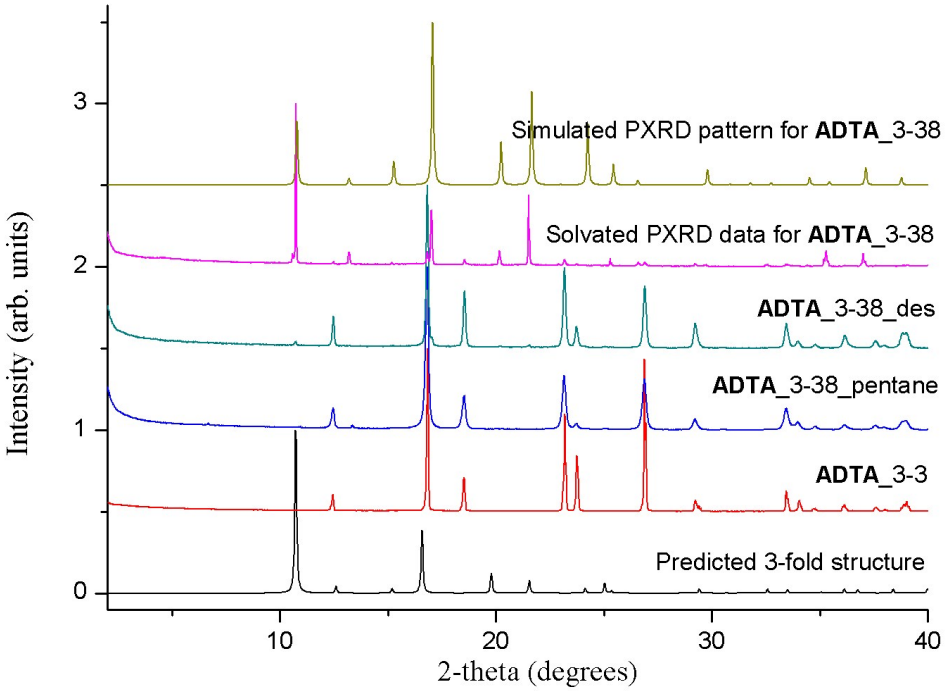

Figure S37. PXRD patterns recorded after activating the **ADTA**_3-38 ethanol/tetradecane solvate: Simulated PXRD pattern of the predicted 3-fold structure (black); simulated PXRD pattern of the experimental 5-fold structure **ADTA**_3-3 (red); experimental PXRD pattern for **ADTA**_3-38 that was recorded after attempting to exchanging the crystallisation solvent with *n*-pentane (blue); experimental PXRD pattern recorded after attempting to desolvate the ethanol/tetradecane solvate, **ADTA**_3-38, at 100 °C under dynamic vacuum (**ADTA**_3-38_des, cyan); experimental PXRD data for fully solvated **ADTA**_3-38 (pink), simulated PXRD pattern from the single crystal structure, **ADTA**_3-38 recorded at 200 K (green).

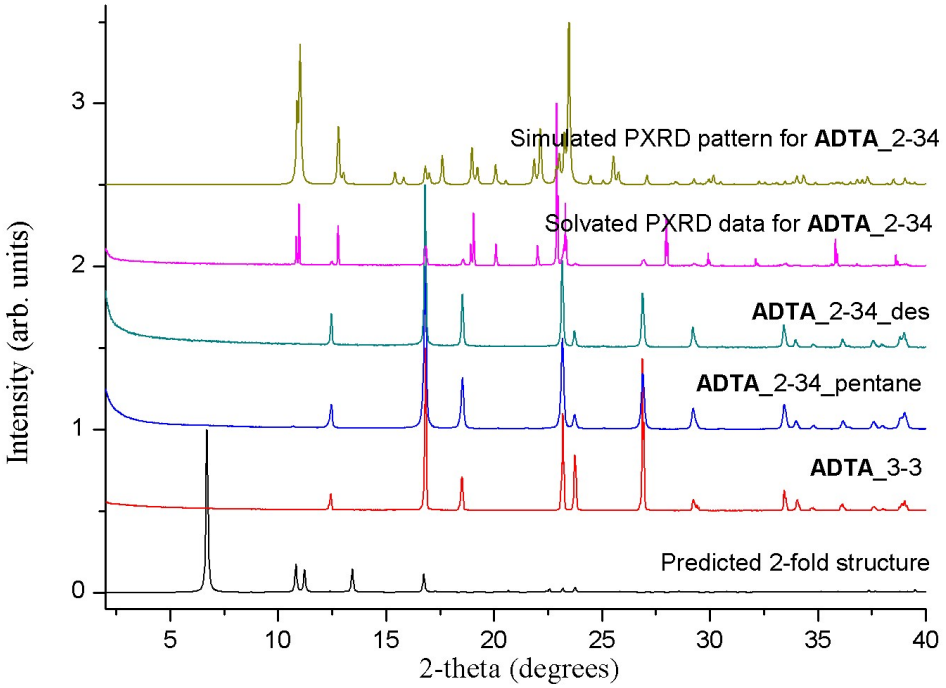

Figure S38. PXRD patterns recorded after activating the **ADTA**_2-34 THF/1,2-dimethoxybenzene solvate: Simulated PXRD pattern of the predicted 2-fold structure (black); simulated PXRD pattern of the experimental 5-fold structure **ADTA**_3-3 (red); experimental PXRD pattern for **ADTA**_2-34 that was recorded after attempting to exchanging the crystallisation solvent with *n*-pentane (blue); experimental PXRD pattern recorded after attempting to desolvate the THF/1,2-dimethoxybenzene solvate, **ADTA**_2-34, at 100 °C under dynamic vacuum (**ADTA**_2-34_des, cyan); experimental PXRD data for fully solvated **ADTA**_2-34 (pink), simulated PXRD pattern from the single crystal structure, **ADTA**_2-34 recorded at 100 K (green).

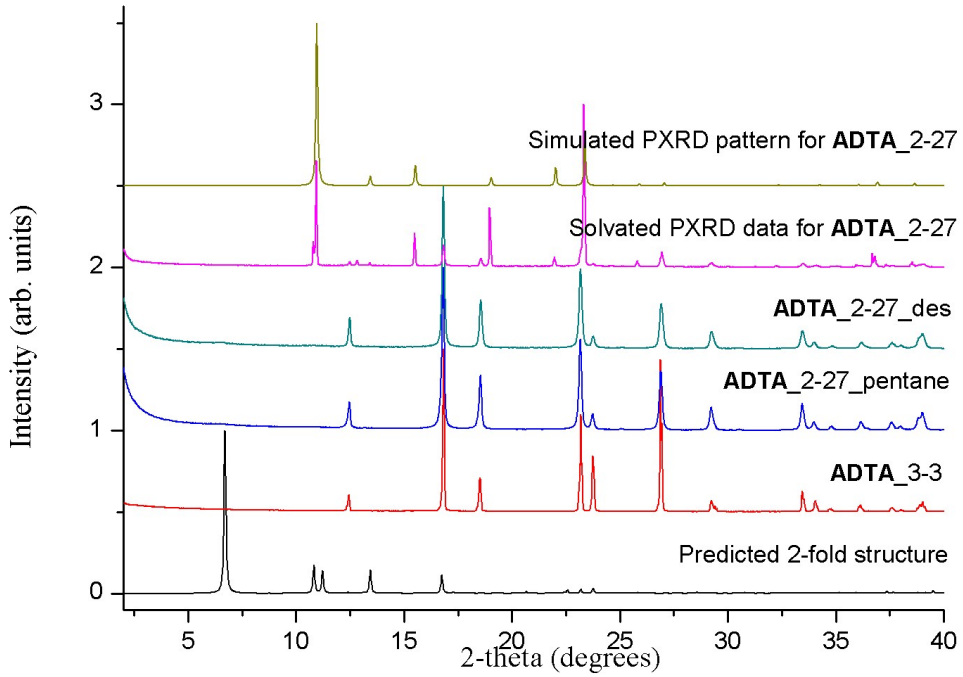

Figure S39. PXRD patterns recorded after activating the **ADTA**_2-27 THF/*o*-xylene solvate: Simulated PXRD pattern of the predicted 2-fold structure (black); simulated PXRD pattern of the experimental 5-fold structure **ADTA**_3-3 (red); experimental PXRD pattern for **ADTA**_2-27 that was recorded after attempting to exchanging the crystallisation solvent with *n*-pentane (blue); experimental PXRD pattern recorded after attempting to desolvate the THF/*o*-xylene solvate, **ADTA**_2-27, at 100 °C under dynamic vacuum (**ADTA**_2-27_des, cyan); experimental PXRD data for fully solvated **ADTA**_2-27 (pink), simulated PXRD pattern from the single crystal structure, **ADTA**_2-27 recorded at 100 K (green).

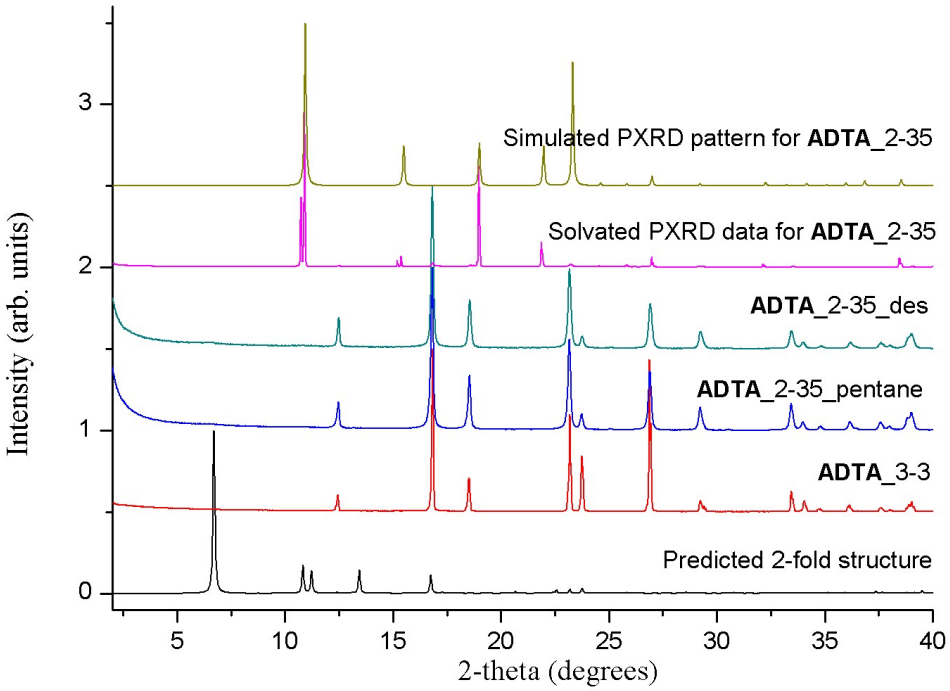

Figure S40. PXRD patterns recorded after activating the **ADTA**_2-35 THF/1,3-dimethoxybenzene solvate: Simulated PXRD pattern of the predicted 2-fold structure (black); simulated PXRD pattern of the experimental 5-fold structure **ADTA**_3-3 (red); experimental PXRD pattern for **ADTA**_2-35 that was recorded after attempting to exchanging the crystallisation solvent with *n*-pentane (blue); experimental PXRD pattern recorded after attempting to desolvate the THF/1,3-dimethoxybenzene solvate, **ADTA**_2-35, at 100 °C under dynamic vacuum (**ADTA**_2-35_des, cyan); experimental PXRD data for fully solvated **ADTA**_2-35 (pink), simulated PXRD pattern from the single crystal structure, **ADTA**_2-35 recorded at 200 K (green).

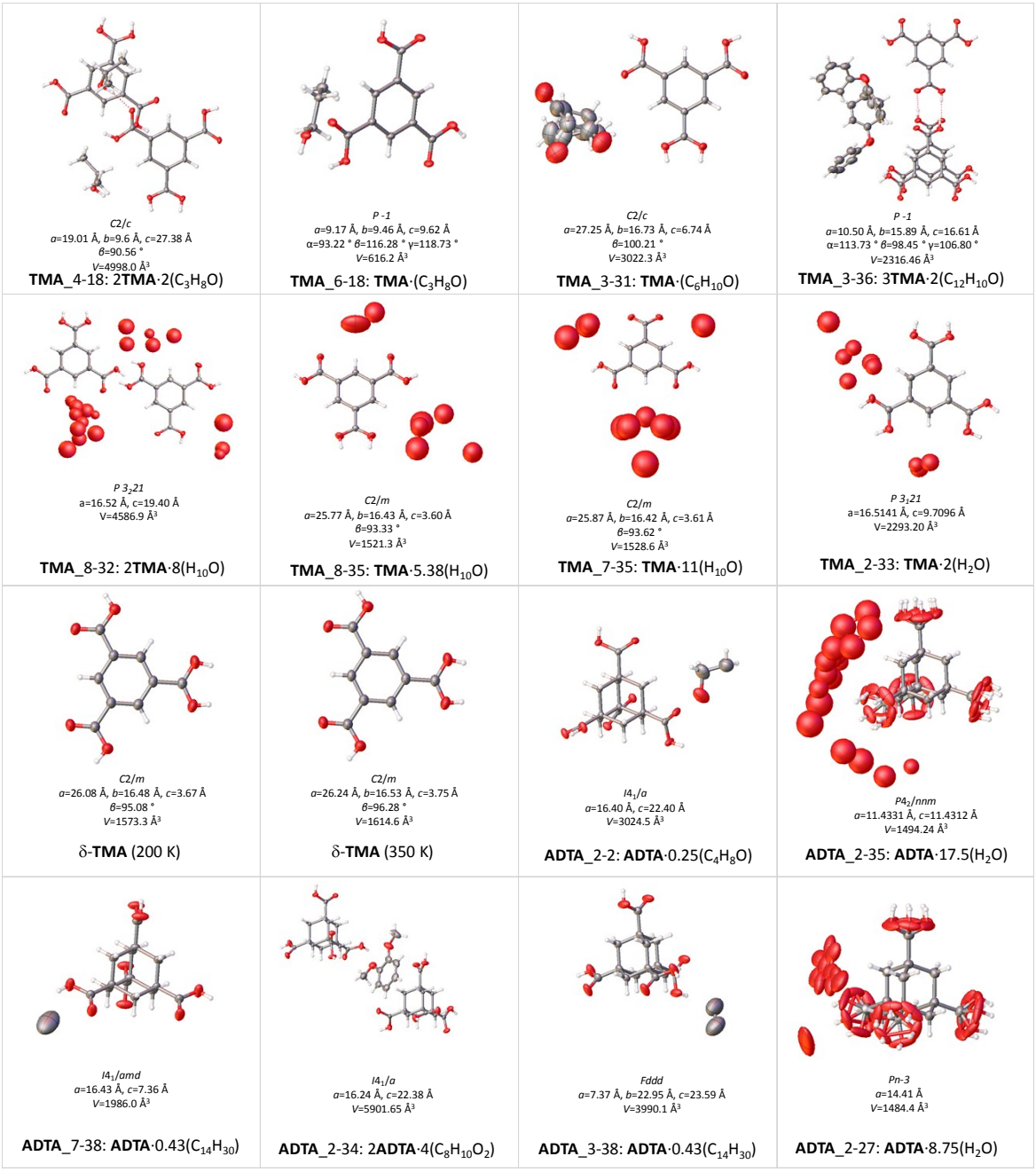

Figure S41. Displacement ellipsoid plots of the asymmetric units from the single crystal structures of **TMA** and **ADTA**. Ellipsoids displayed at 50% probability level. Grey = carbon, white = hydrogen, red = oxygen.

References

1. J. L. Banks, H. S. Beard, Y. Cao, A. E. Cho, W. Damm, R. Farid, A. K. Felts, T. A. Halgren, D. T. Mainz, J. R. Maple, R. Murphy, D. M. Philipp, M. P. Repasky, L. Y. Zhang, B. J. Berne, R. A. Friesner, E. Gallicchio and R. M. Levy, *J. Comp. Chem.* 2005, **26**, 1752.
2. S. Grimme, S. Ehrlich and L. Goerigk, *J. Comp. Chem.* 2011, **32**, 1456.
3. A. D. Becke, *J. Chem. Phys.* 1993, **98**, 5648.
4. P. J. Stephens, F. J. Devlin, C. F. Chabalowski and M. J. Frisch, *J. Phys. Chem.* 1994, **98**, 11623.
5. A. D. McLean and G. S. Chandler, *J. Chem. Phys.* 1980, **72**, 5639.
6. K. Raghavachari, J. S. Binkley, R. Seeger and J. A. Pople, *J. Chem. Phys.* 1980, **72**, 650.
7. M. J. Frisch, G. W. Trucks, H. B. Schlegel, G. E. Scuseria, M. A. Robb, J. R. Cheeseman, G. Scalmani, V. Barone, B. Mennucci, G. A. Petersson, H. Nakatsuji, M. Caricato, X. Li, H. P. Hratchian, A. F. Izmaylov, J. Bloino, G. Zheng, J. L. Sonnenberg, M. Hada, M. Ehara, K. Toyota, R. Fukuda, J. Hasegawa, M. Ishida, T. Nakajima, Y. Honda, O. Kitao, H. Nakai, T. Vreven, J. A. Montgomery, Jr., J. E. Peralta, F. Ogliaro, M. Bearpark, J. J. Heyd, E. Brothers, K. N. Kudin, V. N. Staroverov, R. Kobayashi, J. Normand, K. Raghavachari, A. Rendell, J. C. Burant, S. S. Iyengar, J. Tomasi, M. Cossi, N. Rega, J. M. Millam, M. Klene, J. E. Knox, J. B. Cross, V. Bakken, C. Adamo, J. Jaramillo, R. Gomperts, R. E. Stratmann, O. Yazyev, A. J. Austin, R. Cammi, C. Pomelli, J. W. Ochterski, R. L. Martin, K. Morokuma, V. G. Zakrzewski, G. A. Voth, P. Salvador, J. J. Dannenberg, S. Dapprich, A. D. Daniels, Ö. Farkas, J. B. Foresman, J. V. Ortiz, J. Cioslowski, and D. J. Fox, Gaussian 09, Revision D.01. Gaussian, Inc., Wallingford CT, 2009.
8. D. H. Case, J. E. Campbell, P. J. Bygrave, G. M. Day, *J. Chem. Theory Comput.* 2015, **12**, 910.
9. C. R. Groom, I. J. Bruno, M. P. Lightfoot and S. C. Ward, *Acta Cryst.* 2016, **B72**, 171.
10. S. L. Price, M. Leslie, G. W. A. Welch, M. Habgood, P. G. Karamertzanis and G. M. Day, *Phys. Chem. Chem. Phys.* 2010, **12**, 8478.
11. A. J. Stone, *J. Chem Theory Comp.* 2005, **1**, 1128.
12. D. S. Coombes, S. L. Price, D. J. Willock and M. Leslie, *J. Phys. Chem.* 1996, **100**, 7352.
13. P. J. Winn, G. G. Ferenczy, C. A. Reynolds, *J. Phys. Chem. A*, 1997, **101**, 5437.
14. A. L. Spek, *Acta Cryst.* 2009, **D65**, 148.
15. TOPAS-Academic v. 5 Coelho Software, Brisbane, Australia, 2012.
16. S. Parsons, ECLIPSE. *The University of Edinburgh, Edinburgh, UK*, 2004.
17. G. M. Sheldrick, SADABS. *University of Göttingen, Germany,* 2008.
18. L. Krause, R. Herbst-Irmer, G. M. Sheldrick and D. Stalke, *J. Appl. Cryst.* 2015, **48**, 3.
19. G. Winter, D. G. Waterman, J. M. Parkhurst, A. S. Brewster, R. J. Gildea, M. Gerstel, L. Fuentes-Montero, M. Vollmar, T. Michels-Clark, I. D. Young, N. K. Sauter and G. Evans, *Acta Cryst.* 2018 **D74**, 85.
20. G. Sheldrick, *Acta Cryst.* 2015, **A71**, 3.
21. G. Sheldrick, *Acta Cryst.* 2008, **A64**, 112.
22. G. Sheldrick, *Acta Cryst.* 2015, **C71**, 3.
23. O. V. Dolomanov, L. J. Bourhis, R. J. Gildea, J. A. K. Howard and H. Puschmann, *J. Appl. Cryst.* 2009, **42**, 339.
24. D. J. Duchamp and R. E. Marsh, *Acta Cryst.* 1969, **B25**, 5.
25. F. H. Herbstein, M. Kapon and G. M Reisner, *Acta Cryst.* 1985, **B41**, 348.
26. S. H. Dale and M. R. J. Elsegood, *Acta Cryst.* 2003, **E59**, 127.
27. S. Bernes, G. Hernandez, R. Portillo and R. Gutierrez, *Acta Cryst.* 2008, **E64**, 1366.
28. R. J. Davey, M. Brychczynska, G. Sadiq, G. Dent and R. G. Pritchard, *CrystEngComm,* 2013 **15**, 856.

29. Z. -Z. Fan, X. -H. Li and G. P. Wang, *Acta Cryst.* 2005, **E61**, o1607.
30. F. H. Herbstein, *Acta Cryst.* 1997, **B33**, 2358.
31. S. Chatterjee, V. R. Pedireddi, A. Ranganathan, C. N. R. Rao, *J. Mol. Struct*. 2000, **520**, 107.
32. K. G. Nath, O. Ivasenko, J. M. MacLeod, J. A. Miwa, J. D. Wuest, A. Nanci, D. F. Perepichka and F. Rosei, *J. Phys. Chem. C*, 2007, **111**, 16996.
33. F. H. Herbstein and M. Kapon, *Acta Cryst.* 1978, **B34**, 1608.
34. S. H. Dale, M. R. J. Elsegood, S. J. Richards, *Chem. Commun*. 2004, 1278.
35. M. Sanchez-Sala, O. Vallcorba, C. Domingo, J. A. Ayllón, *Cryst. Growth Des.* 2018, **18**, 6621.
36. S. V. Kolotuchin, P. A. Thiessen, E. E. Fenlon, S. R. Wilson, C. J. Loweth and S. C. Zimmerman, *Chem. Eur. J.* 1999, **5**, 2537.
37. F. H. Herbstein, M. Kapon, and G. M. Reisner, *J. Incl. Phenom.* 1987, **5**, 211.
38. O. Ermer and J. Neudorfl, *Chem. Eur. J.* 2001, **7**, 4961.
39. O. Ermer and J. Neudorfl, *Helv. Chim. Acta,* 2001, **84**, 1268.
40. O. Ermer, *J. Am. Chem. Soc.* 1988, **110**, 3747.